Paleoseismology of the Ganos segment; the western extend of the North Anatolian Fault (Turkey)

MURAT ERSEN AKSOY

MUSTAPHA MEGHRAOUI

MATTHIEU FERRY

ZİYADİN ÇAKIR

GÜLSEN UÇARKUŞ

See next page for additional authors

Paleoseismology of the Ganos segment; the western extend of the North Anatolian Fault (Turkey)

Authors

MURAT ERSEN AKSOY, MUSTAPHA MEGHRAOUI, MATTHIEU FERRY, ZİYADİN ÇAKIR, GÜLSEN UÇARKUŞ, TAYLAN SANÇAR, and MEHMET UĞUR ALTIN

Paleoseismology of the Ganos segment; the western extend of the North Anatolian Fault (Turkey)

**M. Ersen AKSOY[1,4,7,]*, Mustapha MEGHRAOUI[1,2], Matthieu FERRY[3], Ziyadin ÇAKIR[4],
Gülsen UÇARKUŞ[4], Taylan SANÇAR[5], M. Uğur ALTIN[6,a]**

[1]University of Strasbourg, School and Observatory of Earth Sciences (EOST), The French National Centre for Scientific Research (CNRS), Strasbourg, France

[2]University of Strasbourg, Earth and Environment Institute of Strasbourg, The French National Centre for Scientific Research (CNRS), Strasbourg, France

[3]Geosciences Montpellier, University of Montpellier, Montpellier, France

[4]Department of Geological Engineering, İstanbul Technical University, İstanbul, Turkey

[5]Department of Geography, Faculty of Letters, Munzur University, Tunceli, Turkey

[6]Department of Geomatics Engineering, İstanbul Technical University, İstanbul, Turkey

[7]Department of Geological Engineering, Muğla Sıtkı Koçman University, Muğla, Turkey

Abstract: The Ganos fault that ruptured on 9 August 1912 (M_w: 7.4) is the westernmost inland segment of the North Anatolian fault (NAF). Here, the Ganos fault is bounded at its two tips with offshore faults segments, in the Sea of Marmara to the east and the Gulf of Saros to the west in the North Aegean Trough. Therefore, the paleoseismology of the 45-km-long inland fault is of importance to the seismic hazard analysis related to offshore active faults and in particular for the seismic gap in the Marmara Region. Earlier studies have established an earthquake chronology for the western and eastern inland tips of the Ganos fault. Here, we extend the paleoseismic studies toward the central segment. Three trenches at Yörgüç have revealed evidence for two faulting events, possibly post-1669 CE ±30 years, which can be correlated to the 1659 or 1766, and the 1912 historical earthquakes. At Yeniköy, we determined an offset of 46 ± 1 m and 47 ± 1 m on a stream channel and a ridge-crest, respectively. In two trenches we determined two faulting events for the last 1000 years and seven events for the last 3500 years. In trench T5, the base of the displaced stream channel provides a calibrated date of 829–591 BCE. Using the 46 ± 1 m right-lateral displacement, we calculate a slip rate of 16.9 ± 0.7 mm/year for the last 2732 ± 119 years. A combined analysis with earlier paleoseismic studies on the Ganos fault suggests that the historical earthquakes of 1912, 1766b or 1659, 1354 or 1343a, and 1063 ruptured the entire inland fault section. In such a case, the recurrence interval for this section of the NAF corresponds to 283 ± 81 years. Combining earlier estimations, we suggest an average slip rate of 17.1 ± 0.9 mm/year for the last 2700 years and observe a characteristic slip behavior of 4.5 to 5 m per event for this section of the North Anatolian plate boundary fault.

Key words: Paleoseismology, active fault, slip rate, North Anatolian fault, Marmara, Ganos segment

1. Introduction

Determining the magnitude, timing, and recurrence of past large earthquakes and estimating the slip rate of the causative fault are key parameters in providing an earthquake forecast (McCalpin, 2009). The North Anatolian fault is an ideal laboratory to practice such exercise in major continental strike-slip faults. From 1912 to 1999, almost the entire 1500-km-long section of the east-west trending plate boundary fault ruptured with a generally westward-propagating series of earthquakes (Figure 1a; Barka, 1992, 1999; Stein et al., 1997). The traces of the surface ruptures and the geometry of the

ruptured fault segments are still visible (Ketin, 1948, 1969; Ambraseys and Finkel 1987; Ambraseys, 1970; Toksöz, et al., 1979; Barka, 1992, 1996, 1999, Altunel et al., 2004; Aksoy, 2021). Such preserved traces not only allow precise mapping of the fault but permits selecting correct locations for paleoseismic trenching. In addition, the 2000-year-long historical record of destructive earthquakes in Anatolia enables building a seismic event chronology with well-established timing (Sosyal et al., 1981; Guidoboni et al. 1994; Guidoboni and Comastri, 2005; Ambraseys, 2009).

The Ganos segment lies on the western extent of the North Anatolian fault before it enters the North Aegean

* Correspondence: ersenaksoy@mu.edu.tr

[a]The author currently works at BS International Engineering Consulting and Construction Co. Ltd., İstanbul, Turkey

Trough. Its inland fault section is bounded by the Sea of Marmara and the Gulf of Saros on its eastern and western sections, respectively (Figure 1). The Ganos fault ruptured on 9 August 1912 with an earthquake M_w: 7.4 and caused extensive damage in its vicinity. The associated right-lateral coseismic displacement of up to 5.5 m and surface ruptures have been described in contemporary reports and modern studies (Sadi, 1912; Allen, 1913; Hecker, 1920; Mihailovic, 1927; Ambraseys and Finkel, 1987; Altunel and Barka, 2000; Altınok et al., 2003; Altunel et al., 2004; Aksoy et al., 2010; Aksoy 2021).

Recent onshore and offshore investigations suggest that the entire inland section ruptured in both directions with respect to the epicenter; towards the Sea of Marmara
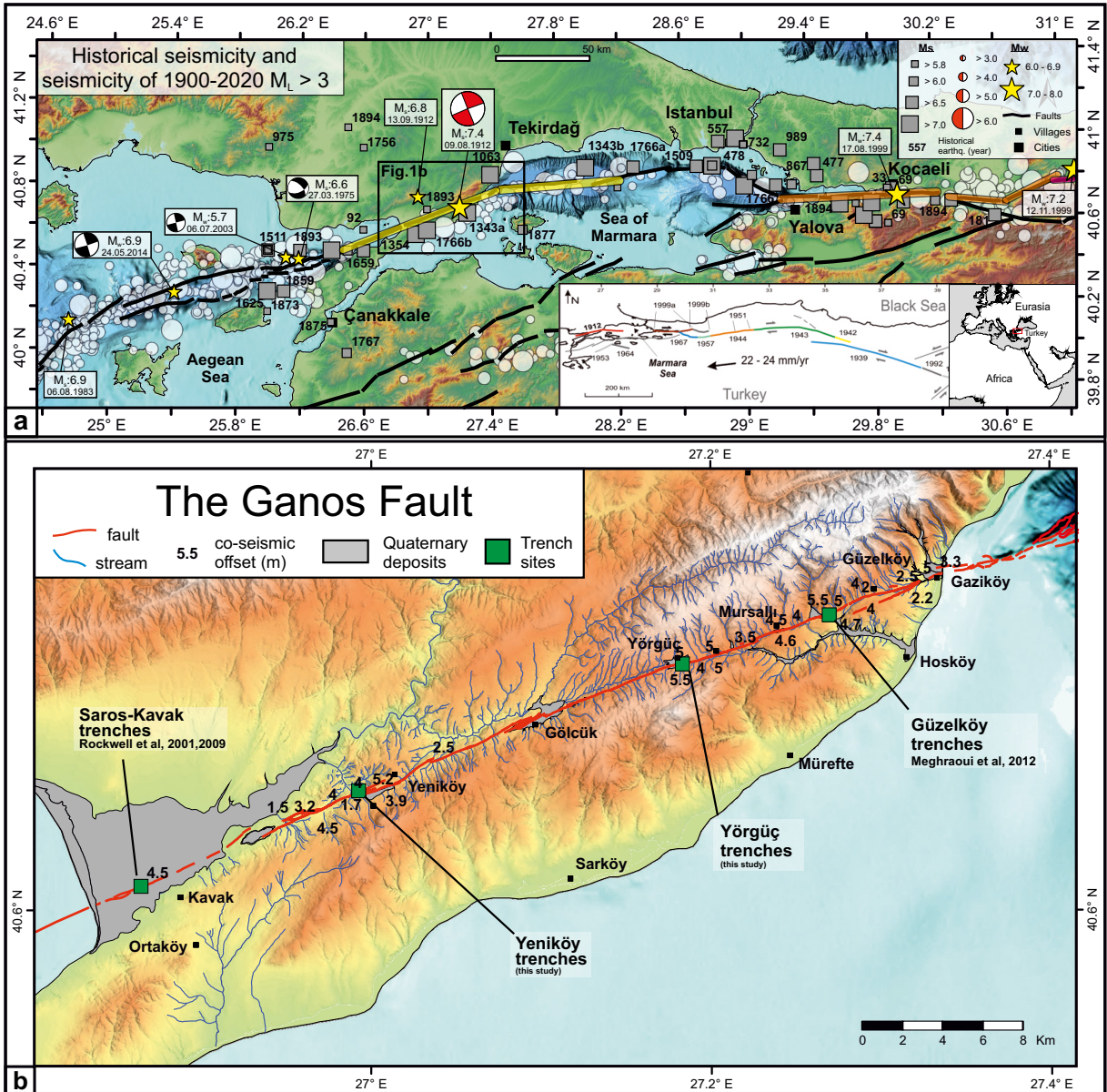
Figure 1. a) Historical (grey boxes) and instrumental (white circles, 1900–2020) seismicity along the NAF in the Marmara Region (source: KOERI, Ambraseys, 2002 and 2009, and Atakan and Sorensen, 2002). Focal mechanisms are from Taymaz et al. (1991), Karabulut et al. (2006), Konca et al. (2018), and Aksoy et al. (2010) for 1912. Black solid lines are active faults. Yellow and orange stripes are the 1912 Mürefte and 1999 Kocaeli earthquake ruptures, respectively (Barka et al., 2002; Çakır et al, 2003; Armijo et al., 2005, Aksoy et al., 2010, 2022). b) The inland section of the Ganos fault segment (red solid line). Sites of paleoseismological studies are indicated with green boxes; Güzelköy (Meghraoui et al., 2012), Saros (Rockwell et al., 2001, 2009), Yörgüç and Yeniköy (this study). Black numbers indicate coseismic offsets (in meters) of the 9 August 1912 earthquake (Altunel et al., 2004; Aksoy et al., 2010; Aksoy 2021).

381

and the Gulf of Saros. The estimated total rupture length is 140 to 160 km (Altunel et al., 2004; Armijo et al., 2005; Aksoy et al., 2010, 2022).

The morphotectonic imprint of successive earthquake faulting is visible along the entire inland fault section with cumulative right-lateral drainage offsets, shutter ridges, sag ponds, and linear scarps. Evidence of past earthquake ruptures has been documented in other earlier paleoseismic studies. Rockwell et al. (2001) opened two trenches at the westernmost limit of the Ganos fault (Kavak) and identified five earthquake event horizons of which the most recent four occurred within the last 1000–1200 years (Figure 1b). In a later trenching campaign in Kavak, Rockwell et al. (2009) revealed evidence of four faulting events after 900 CE. Based on these observations, Rockwell et al. (2009) suggested a recurrence interval of approximately 283 ± 113 years and a slip rate of approximately 16 mm/year for this section of the fault.

On the eastern inland limit of the Ganos fault near Güzelköy, Meghraoui et al. (2012) determined evidence for five paleoearthquakes of which three are after 1311–1397 CE. The recurrence interval calculated from the last four events yields 323 ± 142 years. A slip rate of 17 ± 5 mm/year has been obtained for the last 1000 years.

In this paper, we present new paleoseismic investigations and results for the central section of the Ganos fault segment. We opened five trenches at Yeniköy and three at Yörgüç in 2006 and 2008, respectively. At the Yeniköy trench site, we document a cumulative stream channel offset and a shutter ridge, which allow us to calculate a slip rate for this section of the Ganos fault. Finally, we analyze the earthquake chronology of the entire inland section and suggest an overall recurrence interval and a slip-rate for this segment of the NAF. A supplementary file provides additional figures and tables to support the article.

2. Seismotectonic setting

The inland section of the Ganos fault is 45-km-long and has a highly linear fault geometry. The linearity extends westwards for 37 km into the Gulf of Saros, where the fault bifurcates (Figure 1a, Tüysüz et al., 1998; Yaltırak and Alpar, 2002; Ustaömer et al., 2008; Önder et al., 2021; Aksoy et al., 2022). To the East of the inland section, the Ganos fault forms a restraining bend at the entrance of the Tekirdağ basin and continues eastwards following the margins of the other Sea of Marmara basins (Armijo et al., 2005, Le Pichon et al. 2003, Schmittbuhl et al., 2015).

The present-day seismicity shows a good correlation with the geometrical changes of the NAF in this region with earthquakes clustering at geometrical complexities along the fault (Figure 1a). In the Sea of the Marmara, most of the earthquakes occur where the fault bends (Tamtaş et al., 2021). Similarly the seismicity in the Gulf of Saros is

limited to the west of the fault bifurcation (Karabulut et al., 2006, Konca et al. 2018). The entire linear section of the Ganos fault appears to be aseismic. The lack of seismicity has been attributed by others to the ruptured segment of the 9 August 1912 earthquake (Karabulut et al., 2006, Aksoy et al., 2022).

Historical accounts and seismicity catalogues mention at least 13 destructive earthquakes that may have occurred on the Ganos fault or neighboring segments of the NAF in the last 2400 years (Figure 1; Table 1; Guidoboni et al., 1994; Guidoboni and Comastri 2005; Ambraseys, 2002, 2009). Summaries of these seismic events are available in earlier paleoseismic studies for the Ganos fault and therefore will not be rephrased here (Aksoy, 2009; Meghraoui et al., 2012).

The epicenter locations of historical earthquakes are based on archives with detailed description of damage distribution. Due to their estimated large magnitude some of these earthquakes have possibly ruptured the entire inland section of the Ganos fault and have extended offshore, or may have slipped solely the offshore segments of the NAF. Hence, for a reliable seismic hazard evaluation, determining the causative faults for these historic seismic events requires further investigation. Additionally, we do not know if these earthquakes are comparable to the 1912 event in terms of size and faulting behavior; in other words, if the fault behavior is characteristic or noncharacteristic. Taking into account the uncertainties for this section of the NAF, our paleoseismic analysis on the Ganos fault provides some new constraints for past seismic events along this segment of the plate boundary fault.

3. Tectonic geomorphology

The inland Ganos fault shows a prominent morphology as a linear depression with significant topographic offset along strike. It separates topographic highs to the north and south of the fault (Figure 1b). The linear depression is in general less than 1.5 km wide and signifies a localized deformation along the fault segment. The right-lateral strike-slip motion is well expressed along the entire inland section by pressure ridges, shutter ridges, stream offsets, step-overs with right or left stepping jogs, releasing and restraining bends, back-tilted slopes, and sag ponds (Figure 2, S1; Armijo et al., 1999; Rockwell et al., 2001, 2009; Altunel et al., 2004; Aksoy, 2009, 2021; Meghraoui et al., 2012).

In the East, the Ganos fault runs along the southern slope of the Ganos Mt. (Figure 2). West of Yörgüç, the fault follows the northern limit of the high topography (Figure 1b and 2). Between Yörgüç and Gölcük, the fault is visible as a significant break on the northern hill slopes. Uplifted alluvial fans mark the vertical component of the fault (Figures S1a– S1d).

Table 1. Historical earthquakes in the Ganos region (modified from Meghraoui et al., 2012). References for certain parameters are given below the table.

Date (yr/m/d)	Lat.	Lon.	M_s[a]	I_o	Localities with heavy damage
–360	40.0	26.3	-	-[a]	Çanakkale, Gelibolu
–287	40.3	26.4		-[a]	Çanakkale, Gelibolu, Saros
447.08.25/484.09.00	40.8	29.5	7.2	IX[a,b]	Çanakkale, Gelibolu, Saros
823 (824?).10	40.9	27.4	-	IX[a,b]	Panion (Barbaros), Marmara Ereğli
1063.09.23	41.0	29.0	7.4	IX[c]	Saros, Mürefte, Tekirdağ, İstanbul
1343.10.18a	40.7	27.1	7	VIII[c]	Ganos (İstanbul)
1344.11.06b	40.9	28.0	-	IX[c]	Tekirdağ, İstanbul,
1354.03.01	40.6	26.9	7.4	X[c]	Çanakkale, Gelibolu, Saros, Tekirdağ
1659.02.17	40.5	26.4	7.2	-	Tekirdağ
1766.05.22	41.0	29.0	7.4	-	İstanbul, Bosphorus, Mudanya, Bursa, İzmit, Tekirdağ
1766.08.05	40.6	27.0	7.4	-	Bozcaada, Çanakkale, Gelibolu, Saros, Tekirdağ
1912.08.09	40.7	27.2	7.3	X[d]	Gelibolu, Saros, Tekirdağ
1912.09.13	40.7	27.0	6.9	VII[e]	Gelibolu, Saros, Mürefte

[a]*Ambraseys* [2002, 2009]. [b]*Guidoboni et al.* [1994]. [c]*Guidoboni and Comastri* [2005]. [d]*Ambraseys and Finkel* [1987]. [e]*Hecker* [1920].

4. Paleoseismic trenching

Three earlier trenching campaigns investigated the Ganos fault's paleoseismicity at the eastern and western tips of the inland fault: Meghraoui et al. (2012) and Rockwell et al. (2001, 2009), respectively.

At Kavak, Rockwell et al. (2001) determined five earthquake events of which the most recent four occurred within the last 1000–1200 years. They attributed these events to the historical earthquakes of 824 CE, ca. 1354, 1509, 1766, and 1912. During a second trenching campaign at the same site, Rockwell at al. (2009) documented a 9 ± 1 m displaced buried feeder channel postdating 1655 CE. Four faulting events post-900 CE have been correlated to the 1063 and 1343a or 1354, 1659 or 1766b and 1912 historical seismic events. Rockwell et al. (2009) suggested a recurrence interval of approximately 283 ± 113 years and a slip rate of approximately 16 mm/year assuming the observed 4.5-m coseismic slip for the 1912 is similar in all four earlier events.

On eastern fault section, Meghraoui et al. (2012) show cumulative stream offsets of 10 to 250 m and displaced ridges (Figure 1b). At the Güzelköy trench site, they measure two modern streams displaced for 21.3 ± 1 m and 10.8 ± 0.5 m and a ridge offset of 35.4 ± 1.5 m. 3D trenching allowed measuring a fluvial channel displacement of 16.5 ± 1.5 m. The trenches revealed evidence for five paleoearthquakes (of which the most recent three are post-1311–1397 CE). The last four events have been correlated with 09.08.1912, 1766b or 1659, 1354 or 1343a, and 1063 or 823 historical earthquakes. A recurrence interval of 323 ± 142 years with a characteristic coseismic slip of 5–6 m and a slip-rate of 17 ± 5 mm/year has been suggested for this section of the fault.

In this study, we opened trenches at two sites along the central section of the Ganos fault; at Yörgüç and Yeniköy (Figure 1b).

4.1. Yörgüç trenches

The Yörgüç trenches are located ~1-km-east from Yörgüç village (Figure 2). Here the tectonic deformation is localized within a 10-50-m-wide elongated basin, trending parallel to the fault. Scarps, offset streams and a sag pond allow us to determine the fault location. People in Yörgüç village explain that their elders claimed that the sag pond was created during the 1912 Mürefte earthquake (Figure 2a). Nearby the Yörgüç trenches, earlier studies document 4.0 to 5.5 m coseismic displacement for the 1912 event (Altunel et al., 2004; Aksoy et al., 2010; Aksoy, 2021). We have opened three trenches at this site.

Trench Yr1

The eastern most trench was 1.5 m deep, 15-m-long, and 1.5-m-wide and exposed sedimentary units. Thick layers of loose sand and silt caused instability problems making trench walls collapse at the section where it crossed the fault; the trench could not be logged and was essentially abandoned.

Trench Yr2

We opened a second trench (Yr2) approximately 50 m to the West of Yr1 (Figure 2a). This trench is 50-m-long,
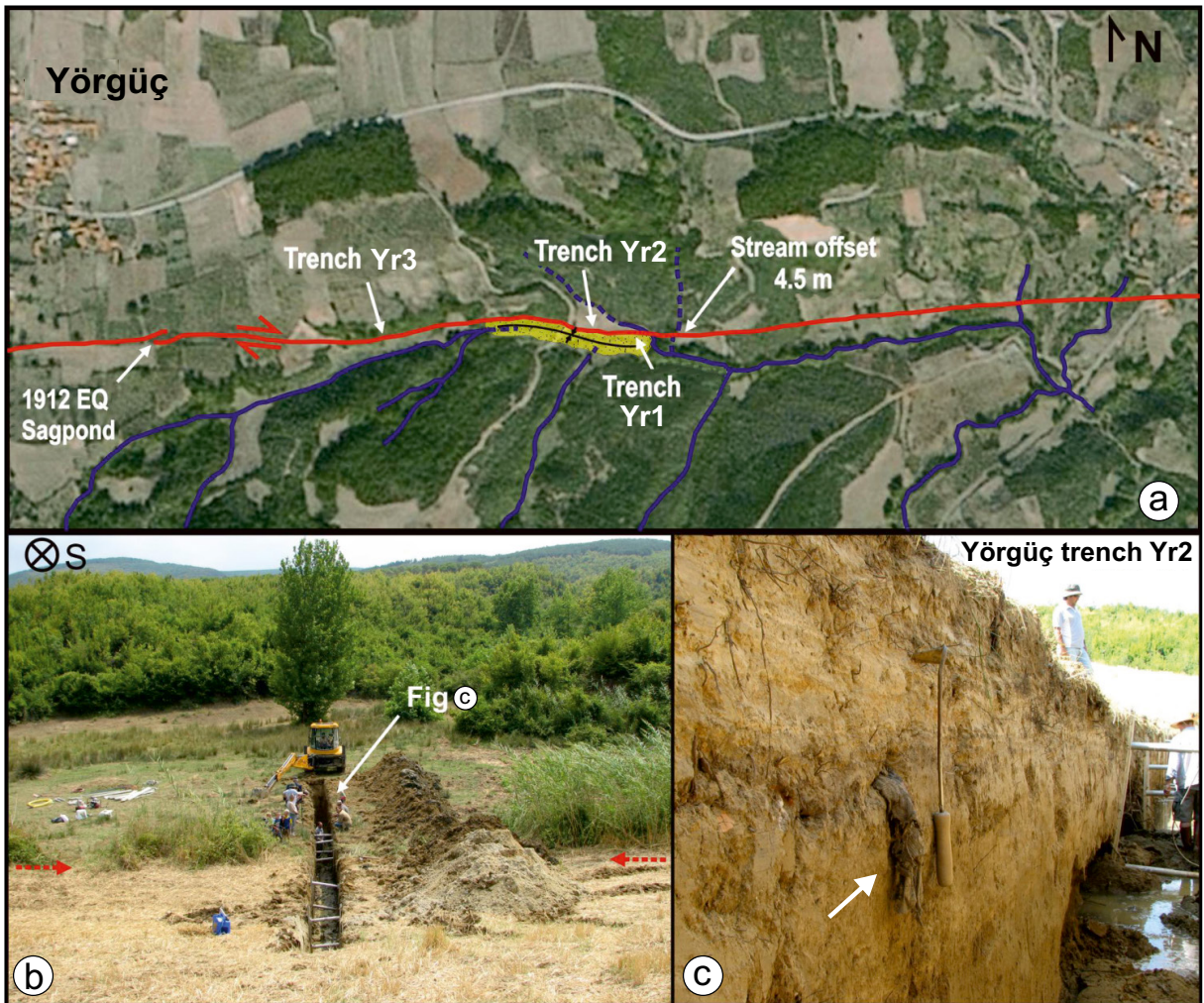
Figure 2. (a) The three trench locations at Yörgüç, (b) Trench Yr2 cross-cut the fault zone and entire valley basin (yellow area in a). (c) The piece of modern cloth at 60 cm depth (see arrow) suggests a recent and rapid sedimentation of unit-e in the area.

1.7-m-deep, and 1.5-m-wide and exposed a wide section of the basin (Figure 2b). The trench walls were stabilized using hydraulic shores. The exposed stratigraphy is composed basically of two series of deposits with an erosional contact in between. The base consists of three units; a, b, and c (Figures 2c and 3). The upper units are silty-clay (unit-d) and clay (unit-e) and overlay unconformably the lower packages (detailed unit description are available in the supplement). At the southern section of the trench, we collected a piece of cloth at nearly 60 cm depth within unit-e. The printings on the fabric suggest a modern age (likely post-1912 event), which would imply a rapid sedimentation.

Within unit-a, a vertically oriented section (a_1) contained a significant number of gravels, which are absent along the other parts of unit-a (Figure 3b). The geometry of unit-a1 and orientation of gravels suggest that the gravels derive from depth and are injected into unit-a due to liquefaction. Due to the geometrical difference between the two boundary sides and sharpness of the southern a-1 boundary, we interpreted that the injection occurred within the fault zone. The scarp on the surface (above the gravels) may support this interpretation but further evidence for faulting is not available. The base of unit-d shows irregularities which resemble flame structures, typical for sand blows. Taking into account the modern age of unit-e, we consider that these structures are most likely related to the most recent 9 August 1912 Mürefte earthquake in the region.

Trench Yr3

Yr3 has been opened further west of Yr2, where the basin gets narrower (Figure 4a). Trench Yr3 is 15-m-long,
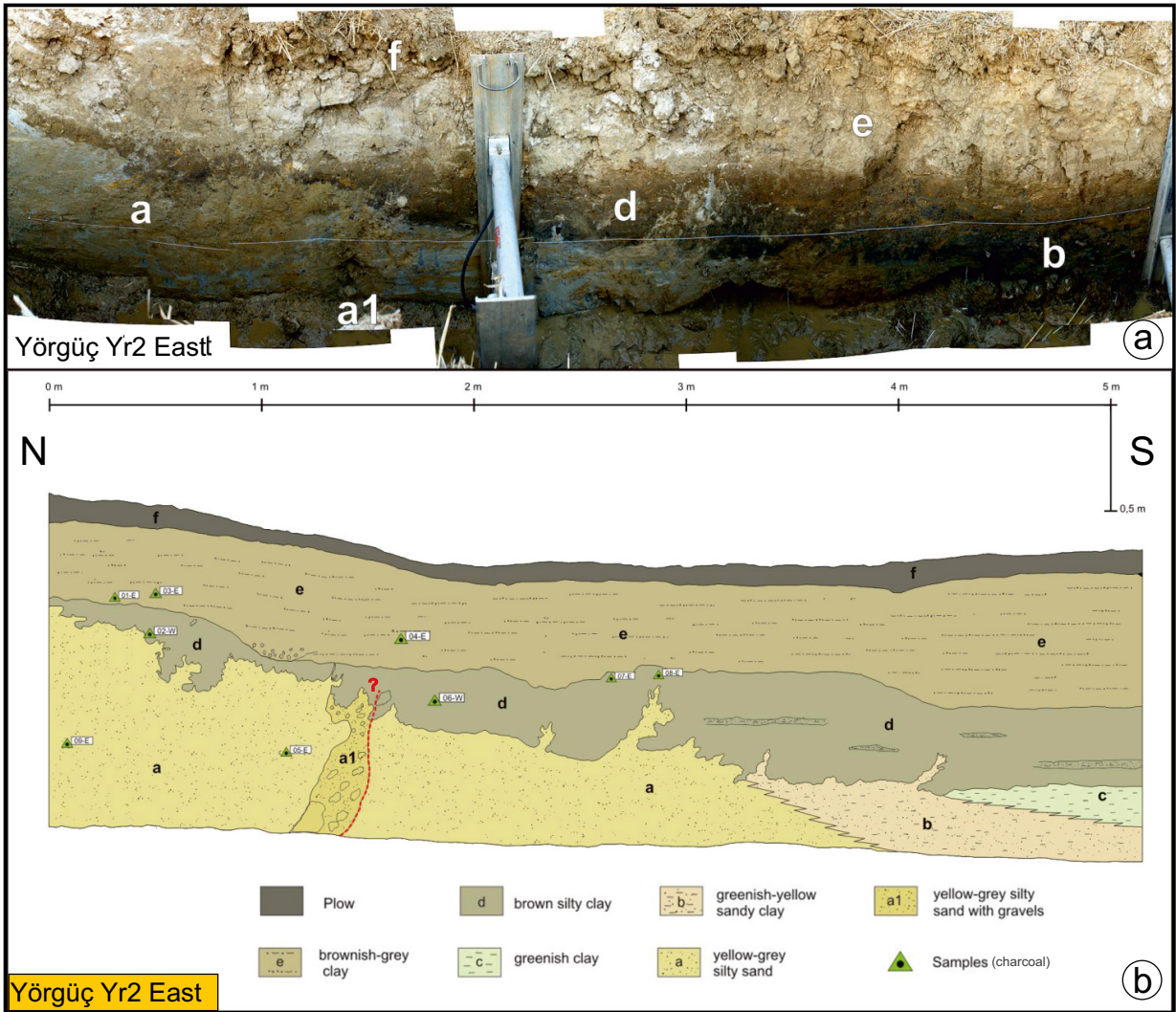
Figure 3. a) Photomosaic of Yr2 east wall. b) Trench log of Yr2. A zone of vertically oriented gravels marks the fault zone. The irregular contact between a and d shows flame structures probably due to earthquake tremor.

3-m-deep, and 3-m-wide and revealed well-stratified sediments (Figures 4 and 5). The trench bottom consists of two packages of clayey silt (units a and b) which is overlain (on an erosional base) by a sequence of clay, silt, and sand; units c to f. The sequence is truncated by erosion and covered the colluvial unit-g and soil (Table S1).

In trench Yr3, a two splay fault affects units a–e (Figure 5). Unit-f overlays the event horizon (green line). Within the splay, an approximately 10 cm vertical displacement is measured affecting units c to e. The fault truncates unit-a. The layer thicknesses on the two sides of the faults for units b to e are different and mark the lateral component of the strike-slip fault. The contrast in thickness for unit-b is significantly larger compared to the other units. This setting suggests that unit-b likely recorded lateral slip

prior to the deposition of unit-c. The amount of slip may correspond to one or more faulting event. Therefore, we assume this setting indicates the existence of at least one more coseismic faulting if not more events (Event 2+).

Calibrated ^{14}C dating results of seven charcoal samples provide some age control. The Oxcal model for samples and event chronology is given in Table 2 and Figure S2 (at 2σ, 95.4% probability; Bronk-Ramsey 2009a; Reimer et al. 2020). Units a and b predate faulting Event 2+. The sample 08-W from unit-b yielded 1682–1913 CE. Unit-c postdates Event 2+. Sample 06-W in unit-c provided an age of 1754–1913 CE at 2σ, while sample 10-W yielded a modern age. Sample 08-W constrains a maximum age of 1682 CE for Event 2+ (single or multiple events). Two samples from unit-e resulted in one modern age and one
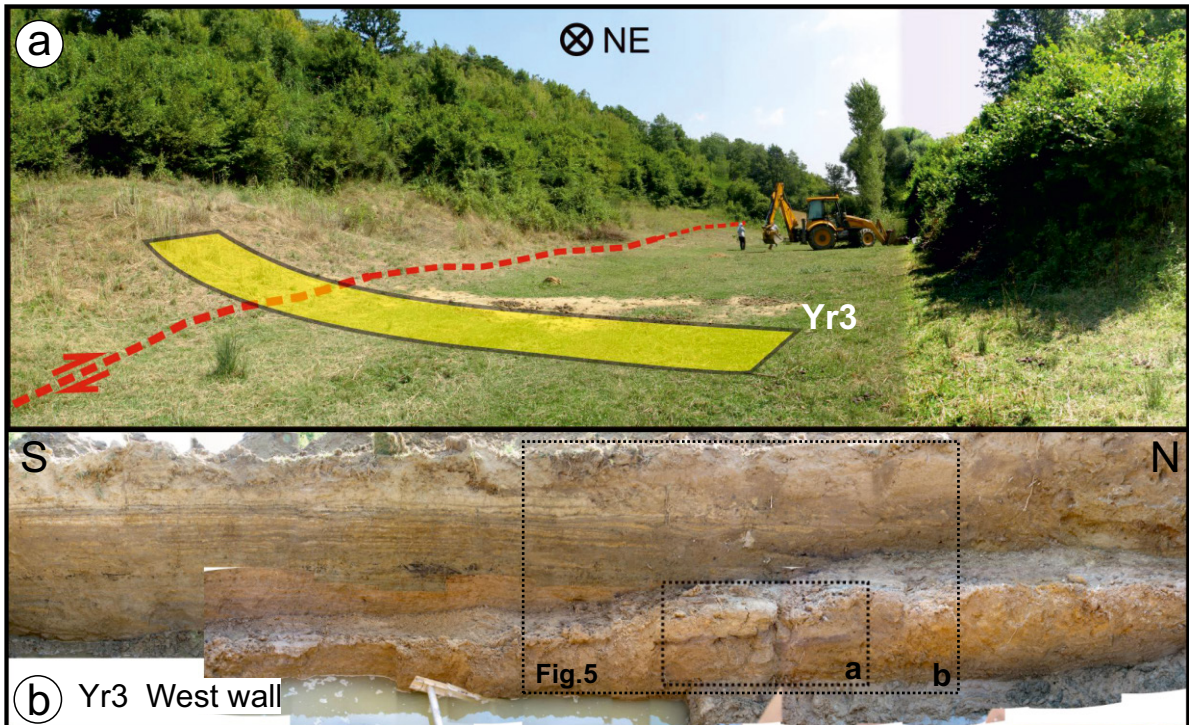
Figure 4. Trench Yr3 is located within a narrow valley parallel to the fault (see Figure 3). The trench was opened across a nearly 2-m-high scarp. (b) The trench stratigraphy showed a fine layered sequence of beds. Near the base of the trench we observe fault branches.

in the range of 1848–1913 CE (YRG-T3-04-W). Samples 06-W and 04-W set an upper limit at 1754–1913 CE. Two samples collected from unit-f yielded modern ages which is consistent with the trench stratigraphy since unit-f corresponds to postevent deposits of Event 1; i.e. the 9 August 1912 earthquake (Figure 8). The Oxcal models suggest an age range of 1771–1913 CE for Event 2+ and post-1843 for Event 1.

4.2. Yeniköy trenches

The Yeniköy paleoseismic site is located 1 km northwest of the Yeniköy village on the central section of the Ganos fault (Figure 1b). Here, the fault makes a 300-m-wide step-over, where the southern branch is bifurcated. Continuous linear escarpments, sag ponds, and cumulative offsets of young streams indicate that the most recent deformation is localized on the northernmost branch (Figures S1g and S1h). On this fault branch (at nearby distances < 1 km), eight offsets on roads, field limits, and streams were identified as coseismic displacements of the 1912 earthquake (Figure 1b; Altunel et al., 2004; Aksoy et al., 2010; Aksoy, 2021).

Geomorphologically, the trench site lies within an N-S trending valley floor; approximately 50-m-wide and entrenched by a small stream (Köy creek) along its eastern margin (Figure 6a). The shoulders of the valley are N-S trending linear ridges. Here, the western ridge crest is

displaced, while the eastern valley slope also shows some amount of deflection. Similarly, the creek flows nearly orthogonal to the fault and shifts rightwards when crossing the fault. Left of the Köy creek lies a 30-m-wide alluvial terrace limited to the north by a fault scarp and related shutter ridge (Figure 6).

We excavated 5 trenches within the alluvial terrace and the western bank of the Köy creek (Figure 6b). Trenches T1, T2, and T4 are across and the other two T3 and T5 are parallel to the fault. Parallel trenches were opened to establish the spatial distribution of a terrace riser that we determined on the left bank of the Köy creek. We logged the trench walls with a 0.5 m grid near and with a 1-m-grid away from the fault. The trench margins, the fault zone limits, stream bed, and the margins of the terrace risers were leveled using a total station.

Yeniköy trench site stratigraphy

Trench T1 is 50-m-long and crosses the entire alluvial terrace (Figures 6 and 7). Layers of loose sand and high groundwater level caused stability problems; therefore, trench depth was limited to 1.5 m and logging was performed only on the west wall. The base of T1 is a colluvial package (a, a_{1-3}) made of mainly silty clay beds (Figures 7 and S3; Table S2). North of the fault, the colluvium is layered and tilted approximately 20° to 30° southward. The 1.5-m-thick colluvium (a_{1-3}) is overlain by
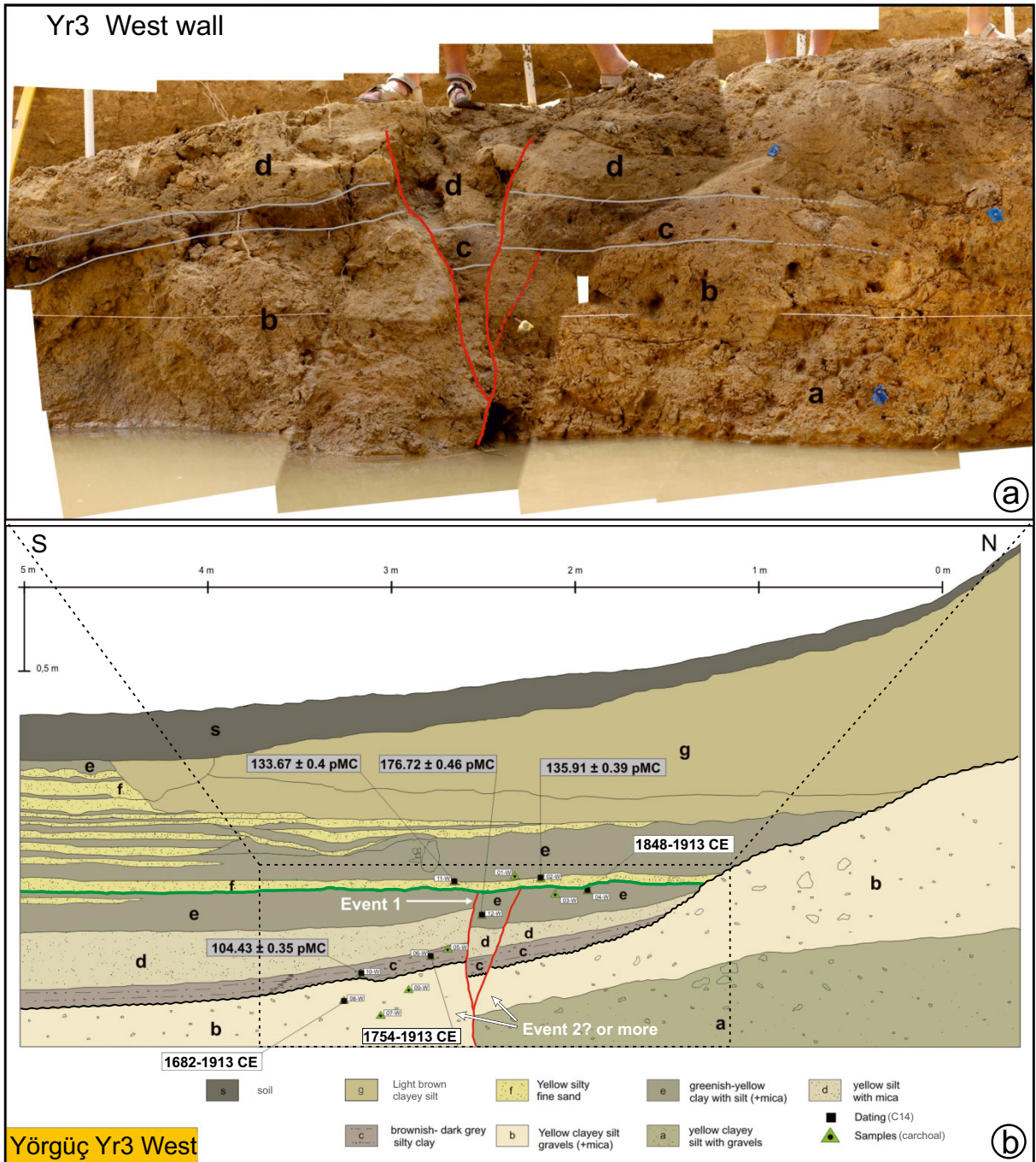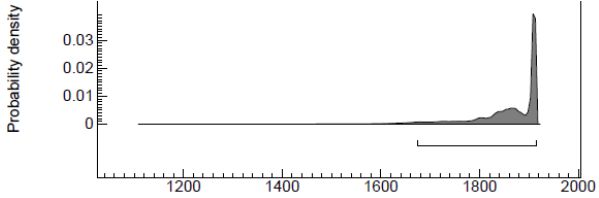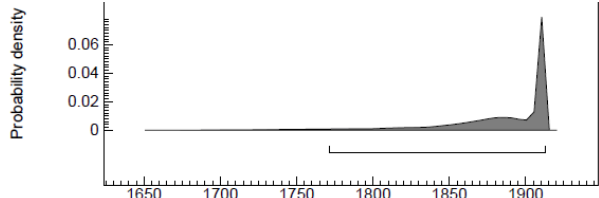
Figure 5. a) Photomosaic of Yr3 trench. b) Trench log. The two splay fault marks the existence of faulting events (see text for details on Event 1 and Event 2? or more). Solid green line is the event horizon of Event 1. Solid black wavy line is an erosional surface. At least one more event can be deduced from the significant thickness difference of unit b, compared to units c, d, e (see text for details).

a reddish clay unit (b). South of the fault, the colluvium (a) is mainly massive and gently dipping to the North. A bluish clayey silt unit (c) is showing liquefaction features. The top of unit (e) and (a) are erosive. Southward, the base of the colluvium (a) is partly interfingering with deposit

(d). Unit (e) rests on top of (d) and is well-stratified with several channels in a northward migrating setting. The uppermost unit of the trench is the soil which may be divided into two sections based on the dominant size of clasts they contain (f_1 and f_2).

Table 2. Calibrated radiocarbon dating results of 7 samples collected from Yörgüç Yr3 (Oxcal and IntCal20 curve Bronk Ramsey 2009a; Reimer et al. 2020). We present here a simulation of age ranges in Oxcal for a possible chronological order of events.

Sample name	Trench unit	Nature	Radiocarbon age (BP)	Uncertainty ± (years)	Unmodelled, calibrated age (+= CE) 2σ range	
YRG-YR3-11-W	f	Charcoal	133.67 ± 0.4 pMC		--	post-1912 EQ
YRG-YR3-02-W	f	Charcoal	135.91 ± 0.39 pMC		--	post-1912 EQ
$E_{1\,(T1)}$, $E_{1\,(YR3)}$					Event 1 (1912)	
					> 1843	
YRG-YR3-12-W	e	Charcoal	176.72 ± 0.46 pMC		--	modern
YRG-YR3-04-W	e	Charcoal	110	30	1682	1938
YRG-YR3-10-W	c	Charcoal	104.43 ± 0.35 pMC		--	modern
YRG-YR3-06-W	c	Charcoal	120	25	1669	modern
$E_{2\,(YR3)}$					Event 2	
					1771	1913
YRG-YR3-08-W	b	Charcoal	145	30	1669	modern

Trench T2 was excavated 20 m westwards from T1. The trench is 22-m-long and 2-m-deep. In trench T2, the lowermost unit is a light-brown massif clay (a) which contains scattered clasts of sandstones with an alternating size of 1–20 cm (Figures 8, 9, S3; Table S2). A bluish unit (b) shows southward tilting (the unit is comparable to (c) in T1). The colluvium (c) overlays conformably (b). A reddish clay unit (d) with some gravels and patches of caliche is deposited on top of (b) with an erosional base. On top of (d), lies a massif wedge-shaped sand deposit (e) which consists partly of pebbles. To the south of the fault, the stratigraphy is different. The base is a massif clay unit (f) with 1–20 cm size scattered gravels. A clayey silt unit (g) rests on top of it unconformably. Further south, (f) is unconformably overlain by an alluvial deposit (h), comparable to (e) in T1. The top of the trench is a 20–40-cm-thick plow package (i).

Trench T3 is 24-m-long and is oriented parallel to the fault. The trench served for tracing the spatial distribution of the terrace riser and draining the high groundwater level in T1.

We did not log the trench but measured the margins of the trench and the terrace riser (Figures 6 and S5).

Trench T4 is 8-m-long, 1-m-deep, and oriented orthogonal to the fault. The trench description and stratigraphy is comparable to T1 and T2 revealing two faults and partly the alluvial deposits and the terrace riser (Figure 10). The base unit is clay (a) and is overlain by several colluvium packages (b). The alluvial deposits (c) are interfingering with the colluviums and indicated a northward migrating sequence as in T1.

Trench T5 is 10-m-long, 2-m-deep, and oriented parallel to the fault. The stratigraphy is similar to T4; with the colluvial and alluvial deposits. Here the alluvial units have been divided into subunits based on the difference of dominant clast size (Figure 10).

Yeniköy sampling and dating results

We have collected 117 samples from the trench units; mostly charcoals and some fragments of wood, ceramic, and gastropod shells. Based on sample quality and stratigraphic position (sample locations are shown on trench logs), we
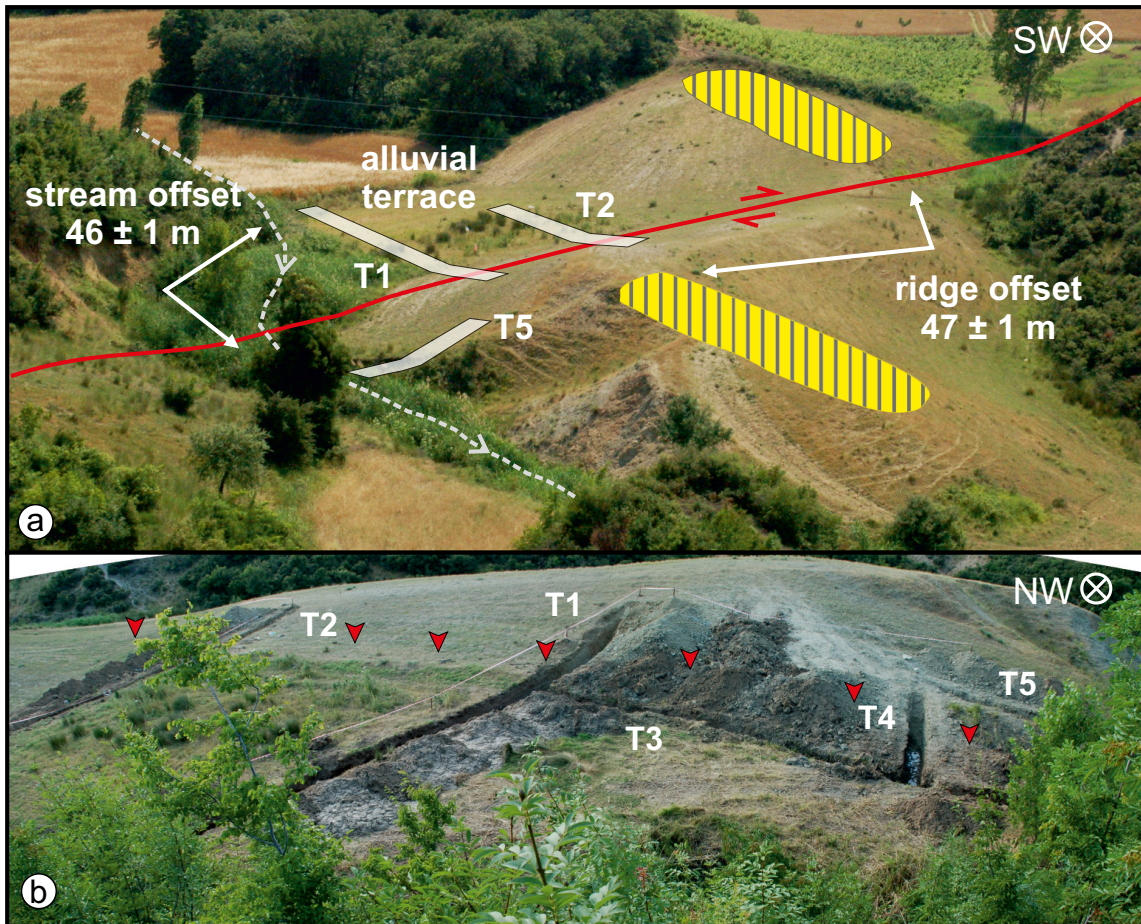
Figure 6. a) The Yeniköy trench site with an approximately 46-m-long cumulative stream offset and an approximately 47-m-long ridge offset. b) Five trenches were dug at this site to reveal the past faulting events of the Ganos fault and to estimate a slip rate at this site. Red arrowheads show the fault trace.

sent 15 detrital charcoal samples for radiocarbon dating (Tables 3 and 4; Figure S4). Sample E59 (T2 east wall) is collected from the uppermost boundary of unit (f) and yields an age of 1493–1796 CE. Samples from the mid-depth of (f) on T2 west wall give an age range of 1500 BCE to 1035 CE. Since these samples may be reworked, they represent maximum ages for unit (f). Three samples from unit (g) provided an age range of 971–1438 CE. The age of sample W46 in unit (e) is significantly old (8620–8304 BCE) compared to other samples.

Yeniköy paleoearthquake analysis and faulting events
Trench T1
We have determined two fault zones in trench T1. The northern section consists of several fault branches (main fault zone), while there are only two fault traces at the center of the trench. The absence of a continuous stratigraphy within the fault zone and existence of erosive limits hinders to comment on the recency of the faulting events. However, cross-cutting relations allowed us to

determine a chronological order and suggest minimum 5, maximum 9 faulting events in this trench. Below is a description of events from youngest to oldest.

Event-1: In Figure 7, the fault F_1 is truncating the uppermost unit (b), (a_3) (a_2), (a_1), and (c). The fault is buried by the youngest soil unit (f_1). Therefore, we assume faulting F_1 is the most recent earthquake rupture exposed on the trench wall.

Event-2: Faults F_2, F_3, and F_4 are overlain by unit (b) and truncate units (a_3), (a_2), and (a_1). F_2 offsets the reddish shear zone of F_3 by 3–5 cm and is necessarily younger than F_3. This setting suggests that F_2 may be the penultimate event in the trench.

Event-3 (+1?): F_3 is displaced by F_2 and is therefore a rupture before F_2 (Event 2). Unit (b) buries F_3 and F_4 and both faults affect (a_1) and (a_2); therefore, F_3 and F_4 may represent a single or two separate events.

Events 4–8: A chronological relation for the remaining faults, F_5, F_6, F_7, and F_8, is problematic because of insufficient
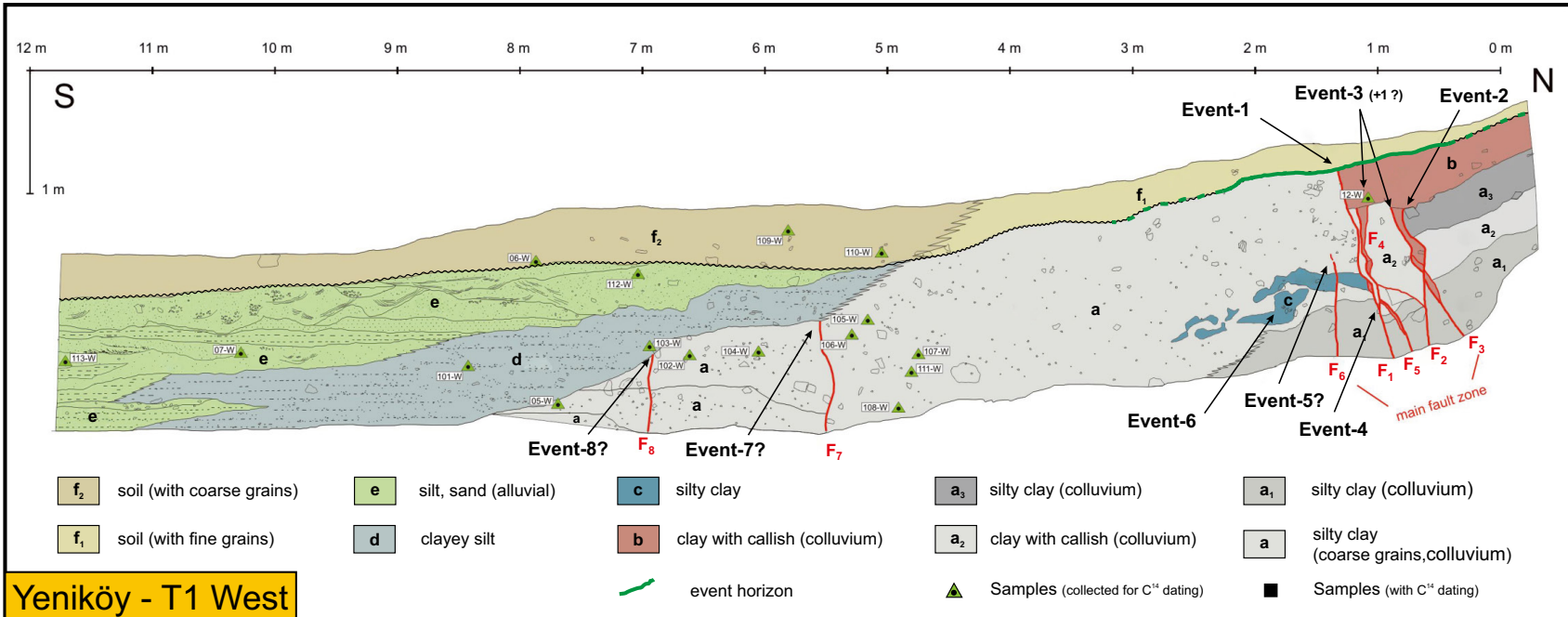
Figure 7. Trench log of west wall of T1 with sedimentary description in Table S2. We observed two zones of faults from 0 to 2 m and from 6 to 7m distance. Faults are red solid lines marked as F1-6.
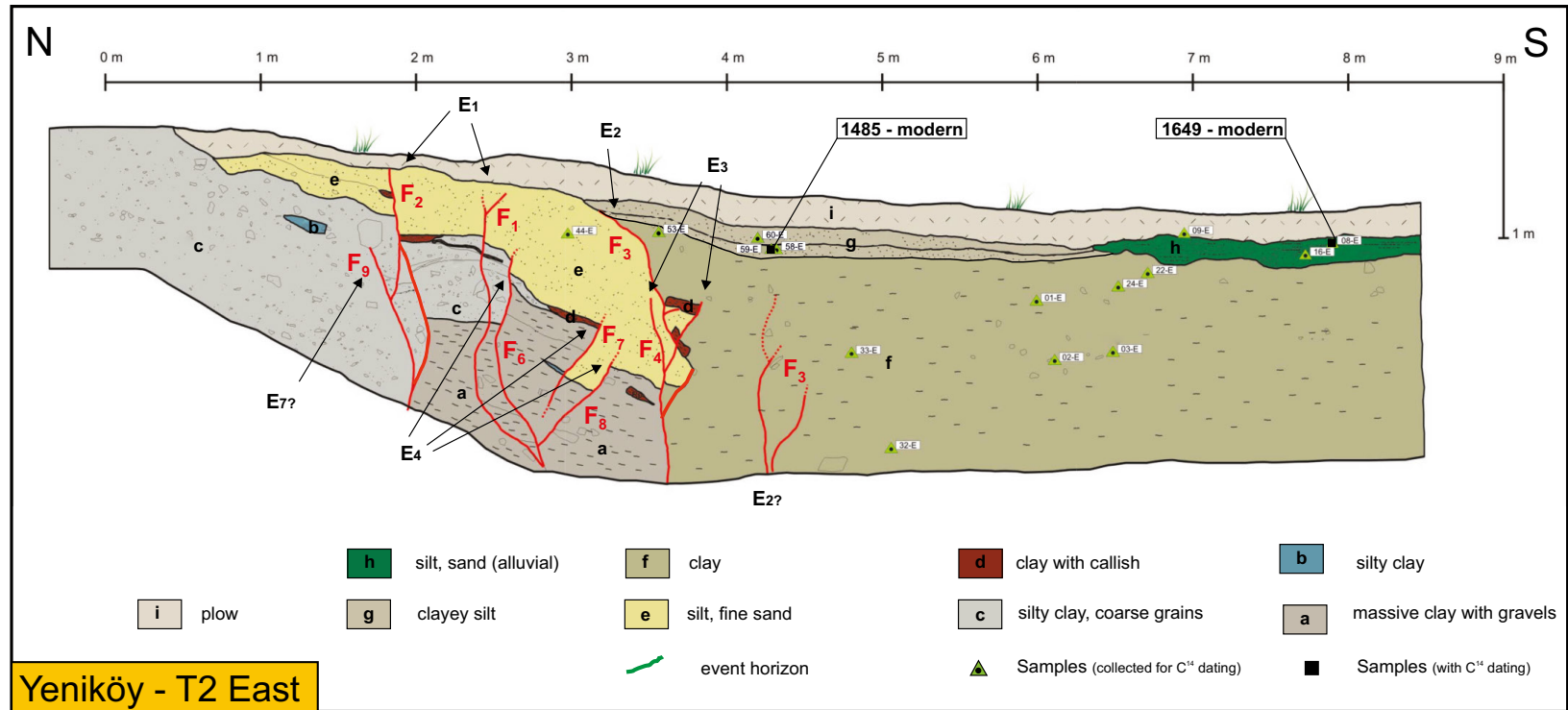
Figure 8. Trench log of the east wall of T2. Faults are red solid lines marked as F1-9. E1-7 represent individual faulting events observed on both trench walls. For missing numbers see the opposite wall. Green triangles are samples collected for dating (charcoal, bulk). Black boxes are samples with radiocarbon ages.

Figure 9. Trench log of the west wall of T2. Faults are red solid lines marked as F1-10. E1-7 represent individual faulting events observed on both trench walls. For missing numbers see opposite wall. Green triangles are samples collected for dating (charcoal, bulk). Black boxes are samples with radiocarbon ages.
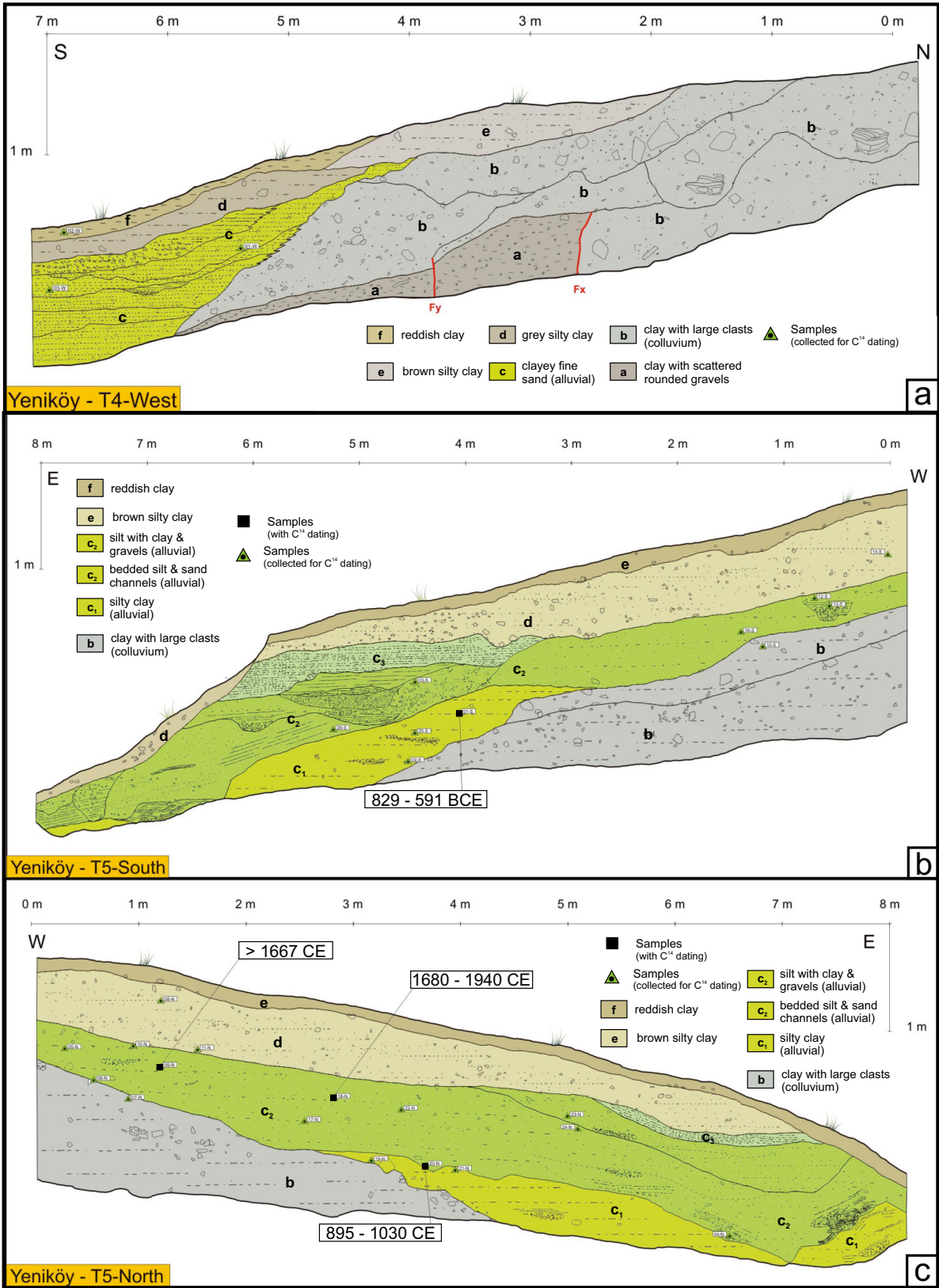
Figure 10. Trench logs of T4 and T5. Faults are red solid lines marked as F. Green triangles are samples collected for dating (charcoal, bulk). Black boxes are dated samples.
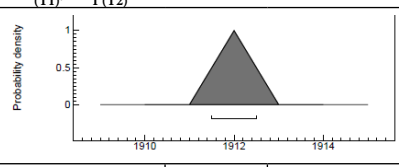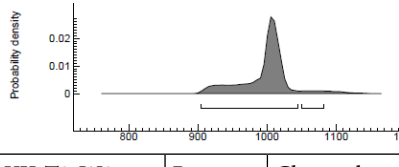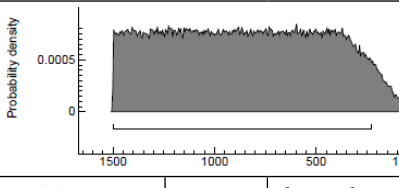
stratigraphy. F_5 consists of a reddish clayey shear zone which is displaced by F_4 near the contact of (a_1) and (a_2). Hence, F_5 is a separate event of F_4. Unit (c) is laterally the equivalent of Unit (b) in T2 West. Unit (b) in T2 is a continuous bed tilting southward, while unit (c) in T1 is disrupted by liquefaction. F_6 offsets the disrupted unit (c). Therefore, we consider that the faulting of a liquefied unit represents two events predating abovementioned events.

F_{6-8} affect unit (a), but F_8 and F_7 are truncated by erosion, therefore likely postdate the colluvium (a) and are younger events than faulting F_6. Assuming these faults represent individual earthquake ruptures, we may suggest minimum 5 or maximum 9 events for T1.

Trench T2

The trench exposed a 4-m-wide fault zone with about ten fault branches and several splays. The stratigraphic and

Table 3. Calibrated radiocarbon dating results of 15 samples collected from Yeniköy T2 and T5 using Oxcal (Bronk Ramsey 2009a and IntCal20 curve (Reimer et al., 2020). We also simulated with Oxcal the age ranges for a possible chronological order of events.

Sample name	Trench unit	Nature	Radiocarbon age (BP)	Uncertainty ± (years)	Unmodelled, calibrated age (+= CE) 2σ range	
E1 (T1), E1 (T2)					Event 1	
					> 1660	
YK-T2-E08	Flv	Charcoal	190	30	1649	modern
YK-T2-E59	Sc	Charcoal	250	50	1485	modern
YK-T2-W55	Sc	Charcoal	540	30	1322	1437
YK-T2-W28	Sc	Charcoal	1060	30	895	1030
E2 (T2)					Event 2	
					905	1049
YK-T2-W05	Brsc	Charcoal	1015	30	987	1153
YK-T2-W31	Brsc	Charcoal	2150	60	−372	−44
YK-T2-W34	Brsc	Charcoal	2770	35	−1004	−830
YK-T2-W61	Brsc	Charcoal	2985	30	−1376	−1116
YK-T2-W04	Brsc	Charcoal	3130	50	−1501	−1273
E2-E6 (T1), E3-7 (T2)					min 7, max 9 events	
						< -1103
YK-T2-W46	Ysc	charcoal	9250	60	−8620	−8304
Trench 5						
YK-T5-N18	Bc	charcoal	115	30	1680	1940
YK-T5-N09	Bc	charcoal	150	30	1667	modern
YK-T5-N20	Rsc	charcoal	1060	30	895	1030
YK-T5-S01	Rsc	charcoal	2600	35	−829	−591

Table 4. A summary of faulting events observed in the Yeniköy trenches. Faults (ruptures) and units are given in relation with the trench logs (Figures 7–9). The absence of comparable stratigraphy did not allow a cross-correlation for events among trenches T1, T2, and T4 (except for event-E1).

Event	T1 West	T2 West	T2 East	Predating unit T1/T2	Postdating unit T1/T2	^{14}C dating
E1	F1	F1, F2, F3	F1, F2	a,b,e / g	f / i	post-895 CE
E2	?	F4, F5, F6	F3	a_{1-3}, b, c / g	b / i	post-987 CE
E3	?	F7	F5	- / a,e	e	-
E4	?	-	F6, F7, F8	- /d,e	e	-
E5	?	F8	-	- / c,b	e	-
E6	?	F9	-	- / c	d	-
E7	?	F10	-	- / c	c	-

structural order of units is comparable to T1, except for unit-e. The juxtaposed units (e, c, f) suggest successive strike-slip faulting. The trench shows evidence of at least 7 surface rupturing events (Figures 8 and 9; Table 4).

Event-E$_1$: On the western wall, three fault splays F$_1$, F$_2$, and F$_3$ rupture all units but the plow unit (i). Fault F$_1$ affects unit (g) and is covered by unit (i). Similarly, on the eastern wall, F$_1$ and F$_2$ truncate all units except unit (i). The base of the plow (i) buries F$_1$; therefore, the event is bracketed between (g) and (i) and represents the most recent event in the trench. Three charcoal samples from unit-g yield calibrated ages of 1485–modern CE (E59), 1322–1437 CE (55-W), and 895–1030 CE (28-W). Hence the faulting event age lies between 895 CE to modern and corresponds to a maximum age for E1. The event horizon is younger since samples are from the mid-depth of the unit, and likely corresponds to the 9 August 1912 earthquake.

Event-E$_2$: On the west wall, faults F$_4$, F$_5$, and F$_6$ affect units (f) and (e) and are buried by unit (g). On the east wall, F$_3$ truncates (a), (f), (e), and (d) and terminates at the base of (g). Units (i) and (g) postdate these faults. The base of (g) is erosional; therefore, we are not able to build a chronology among F$_3$ on the east wall and F$_4$, F$_5$, and F$_6$ on the west wall. Hence, we assume the faults correspond to a single event and represent the second youngest earthquake rupture in this trench. Unit (g) buries these events, therefore setting an upper boundary at 895-modern for the event. The event postdates (f) for which radiocarbon ages yield a range of 1501 BCE to 987 CE. Among these samples, W04, W61, and W34 are at middepth and close to each other. The samples provided much older ages relative to other samples at the same and lower depth (W05, W31). The ages of W31 and W05 are consistent in stratigraphic order and likely provide a better age constrain for (f) (372 BCE to 1153 CE). The upper sample is W05 dating 987–1153 CE and represents a maximum age for event E2.

Another fault F$_4$ on the east wall affects unit (f) and terminates within the unit. The faulting may be compared to the fault branches F$_{4-5}$ on the west wall but may also represent a different faulting event that occurred during the deposition of unit (f).

Additional events (with no age control):
We observed other fault branches truncating the colluvial units on both trench walls. The colluvial units are lying below an erosional surface; the base of the plow (i) and unit (g). The absence of a continuous stratigraphy limits establishing the timing of additional faulting events. However, cross-cutting relations allow building a relative chronology among ruptures.

Event-E3: Rupture F$_7$ on the west wall affects units (a) and (e), and is covered by the upper section of (e). Therefore, F$_7$ can be considered an extra event: Event E3. A similar setting can be observed on fault F$_5$ on the east wall, where a branch terminates within unit (e).

Event-E4: On the east wall, ruptures F$_6$, F$_7$, and F$_8$ displace units (a) to (e). Since these faults affect only the base of unit (e) and do not reach the younger parts of (e) like E3, the faults can potentially correspond to another event older than E3. A similar setting (event) is not observed on the west wall.

Event-E5: On the west wall, F$_8$ ruptures and offsets units (a), (b), (c), and the tip of (b) but does not affect (e). Therefore, this rupture is considered a separate event compared to E4, postdating unit (d) and predating unit (e).

Event-E6: On the west wall, F$_9$ offsets units (a) and (b) and the base of (c) but terminates at the base of (d). Since the faulting predates (d), it is necessarily a separate event.

Event-E7: On the west wall, F$_{10}$ affects units (a) and (b) and the base of (c). The faults terminate within the lower section of the colluvium (c) and therefore suggest that the faulting occurred during the deposition of (c). Thus, it is considered an event prior to E6. The stratigraphy is

insufficient to clarify an equivalent faulting on the east wall. However, fault F9 (east wall) may be a possible candidate, if it is not an individual faulting event.

The absence of a continuous and comparable stratigraphy among trenches T1, T2, and T4 hinders a correlation of events. Nevertheless, cross-cutting relations suggest minimum 5 or maximum 9 events for T1 and at least 7 events for T2. An age control was only possible for the most recent two events in T2 (Tables 3 and 4; Figure S4)

Yeniköy Stream offset and slip-rate estimation
At the Yeniköy trench site, an N-S trending linear ridge shows right lateral slip (Figures 6a and S5). A comparable offset is determined on the Köy creek that flows nearly orthogonal to the fault. Using a differential GPS station, we built a 0.5-m resolution digital terrain model (DTM; based 5500 topographic points) of the site (Figure S5). The projection of the linear hill crests onto the fault shows 47 ± 1 m of right-lateral displacement. The southern section of the Köy creek flows nearly orthogonal to the fault strike. Approaching the fault, the streambed deflects towards the right. North of the fault, the northernmost valley section is also linear and oriented orthogonal to the fault. Projecting these two sections onto the fault yields 46 ± 1 m of right-lateral displacement, comparable to the ridge offset. In addition, east of T1, we observe on the stream bank a terrace riser trending NNE, which is continuous until the fault. We opened trenches T3, T4, and T5 to map the fluvial deposits related to the riser on the both sides of the fault (Figure 10). In trench T3, we surveyed the location of the riser but did not perform any logging because the trench served also as an outlet channel to drain the high groundwater in T1.

We followed the riser in trench T4, where we determined two fault splays (Figure 10a). The stratigraphy of T4 is similar to T1 and T2, where the bottom unit is the clay unit (a) and is covered by a sequence of colluvial deposits unit (b). The alluvial deposit unit (c) interfingers with the colluvium (b) and shows a northward migrating sequence as observed in T1.

The stratigraphy in T5 consists of a colluvial basement unit (b) overlain by a westward migrating channel sequence. We exposed the base and nearly the lowest sediments of the Köy creek, which allowed determining an age for the streambed (Figures 10b, 10c, and S4). Radiocarbon dating (2σ) from unit Fbc (sample 20-N) and Fsc (sample 01-S) yield calibrated calendar ages 895–1030 AD and 829–591 BCE, respectively. Sample 01-S is taken nearly from the top of unit Fsc and gives a minimum age of 2716 ± 119 years for the channel. Within 1σ range, 89.9% lies between 829 and 752 BCE, suggesting a most probable age of 2797 ± 39 years. Taking into account the 46 ±1 m right-lateral offset and the age of the channel, we may deduce a maximum

slip-rate of 17.0 ± 0.7 mm/year or 16.5 ± 0.2 mm/year for the last 2716 ± 119 years or 2797 ± 39 years, respectively.

5. Discussion
Our paleoseismic investigation at Yörgüç and Yeniköy sites of the Ganos fault provide new findings along the westernmost inland section of the North Anatolian plate boundary fault. Here we discuss our results, examine earlier trenching studies and provide a combined analysis on the paleoseismology of the Ganos fault section of the NAF.

Yörgüç trenches
The Yörgüç trenches showed evidence of liquefaction and minimum two faulting events.

The trench Yr2 is 50-m-long and cross-cuts almost the entire depression; nevertheless, we observed no surface ruptures except a vertically oriented zone of gravels. Our trench either missed the fault or it is located deeper. On the other hand, the contact of units a, b, and d in Yr2 shows flame structures. The overlaying unit e is undisturbed. The newness and the imprinting on the fabric we found within unit e implies a modern age for the unit (tentatively post-1950s, but likely younger). The lithological similarity of units e and d indicates that they have been deposited in the same environment and their ages are comparable. Thus, we may assume that the age of unit d is very young and the liquefaction structures can be attributed to a very recent, significantly large earthquake (M ≥ 6) in the region. There are three known shocks in the area that could cause such phenomena; the 9 Aug. 1912 (M_w 7.4), 10 Aug. 1912 (M_w 6.2), and 13 Sept. 1912 (M_w 6.9).

In trench Yr3, the two fault splays are buried by a sequence of sand (f) and clay (e) alternation. The fault affects the base of this sequence; it offsets the lowermost e and is overlain by unit f. All samples from the two units yield modern ages, supporting that the rupture is a very recent event, such as the 9 Aug. 1912 earthquake. The fault disrupts units c, d, and e. The thickness of the units remain similar on both sides of the faults suggesting that 5 to 10 cm height differences are related to the vertical throw of the fault. Earlier studies measured up to 5.5 m coseismic lateral displacement for the 9 Aug. earthquake at very close locations to the trench site (Altunel et al., 2004; Aksoy et al., 2010; Aksoy 2021). Assuming the faults in Yr3 are related to the 9 Aug. event, such extensive displacement is likely accompanied with larger throw values since the trench site lies morphologically in a linear depression. Therefore, it is possible that the trench exposed only a branch of the main rupture; therefore, less slip is observed. The main rupture could be located slightly further north along the steep slope foot.

Yeniköy trenches
The Yeniköy trenches reveal fault zones with several fault branches, from which we determine 7 to 9 events. The

lack of a continuous stratigraphy overlaying the fault zone hindered the possibility of constraining a timing for the faulting events. Nevertheless, some sedimentary layers and crosscutting relations allowed building a chronology among the fault branches. The most recent event in T2 is postdating unit (g) for which radiocarbon dating yielded a date of 895 CE to modern (Table 3). The penultimate event is bracketed by the ages of units (g) and (f). Charcoal samples from unit (f) provided a wide age range (1500 BCE to 1153 CE). The ages for samples 31-W and 05-W are compatible with the stratigraphy and of (g). Samples 61-W, 34-W, and 04-W are close to each other, stratigraphically slightly above sample 05-W and close to the fault zone and therefore are more likely to get contaminated. Therefore, we assume the samples represent a maximum age for the unit. Sample 05-W represents a better lower limit for the penultimate event (post-987–1153 CE). At least 5 more events have been determined in T1 and T2. These events truncate unit (e) (8620-8304 BCE), but we consider that sample 46-W is most likely contaminated and provides a maximum age for the unit.

Correlation with historical seismicity

The historical earthquakes in the Ganos region are the 1063 (M_s: 7.4) with epicenter south of Tekirdağ, the 1343a (M_s: 7.4) with epicenter west of Tekirdağ, the 1354 (M_s 7.4) with epicenter near Şarköy, the 1659 (M_s: 7.2) with epicenter in the eastern part of the Gulf of Saros, the 1766b (M_s: 7.4) with epicenter near Şarköy and the 9 August 1912 (M_w 7.4) with epicenter north of Mürefte (Table 1 and Figure 1a). The estimated magnitudes of these earthquakes imply that they caused surface ruptures on the Ganos fault or neighboring segments.

Combining the paleoseismic results of Rockwell et al. (2001, 2009) and Meghraoui et al. (2012) four trench sites show evidence of four faulting events on the Ganos fault for the last 2000 years (Figure 11). Combining with their 2001 study, Rockwell et al. (2009) suggests that the four events at Saros correspond to the 1063, 1343a or 1354, 1659 or 1766b, and the 1912 historical earthquakes and calculates a 280 ±110 year recurrence interval for this section of the fault. In Güzelköy, Meghraoui et al. (2012) shows traces of five faulting events post-79 CE, relates them with the 823 or 1063, 1343a or 1354, 1659 or 1766b and 1912 historical earthquakes, and suggest a recurrence interval of 323 ± 142 years for M > 7 earthquakes.

Uniting all paleoseismic results, we are able to constrain the chronology for the last four events along the Ganos fault. Figure 11 summarizes the spatiotemporal distribution of the events. We deduce the following results: 1) The 1063, 1343a, 1354, 1659, 1766b, and the 1912 earthquakes were large earthquakes (M_w > 7.2) associated with surface ruptures. 2) The 45-km-long inland Ganos fault section ruptured during the 1063, 1343a or 1354, 1659 or 1766b, and the 1912 earthquakes. The sequential earthquakes of

1343a/1354 and 1659/1766b are problematic. According to historical sources (Guidoboni et al., 1994; Ambraseys 2002, 2009; Guidoboni and Comastri, 2005), the 1766b and 1659 earthquakes caused damage in the Ganos region, but the damage of 1766 extends eastwards towards İstanbul and of the 1659 extends towards the Gulf of Saros. Similarly, the 1354 affected the Ganos and Saros and the 1343 the Ganos and Tekirdağ regions. Paleoseismic analysis along the Ganos fault show that these consequent earthquakes in each sequence did not rupture the same fault sections and occurred on neighboring fault segments. 3) We suggest two chronological scenarios (Scn) for the historical earthquakes (Table 5). According to Scn-1, the Ganos fault ruptures with comparable interseismic periods (253–310 years) in favor with characteristic fault behavior (i.e. M_w 7.4 comparable to the 1912). In Scn-2, the interseismic periods shows variation from 146 to 418 years and suggests a mix between characteristic (M_w > 7) and noncharacteristic fault behavior (M_w ≤ 7). Ambraseys (2002) attributes the 1766 earthquake to the Ganos fault. However, other studies suggest an offshore location in the Sea of Marmara (Altınok et al., 2003). In Scn-2, the interval between 1766 and 1912 is nearly 50% shorter than the suggested recurrence interval. Taking into account the approximately 24 mm/year GPS velocity for the western part of the North Anatolian Fault (Reilinger et al., 2006) and the 16 to 22 mm/year geologic slip rates for the Ganos region (Rockwell et al., 2009, Meghraoui et al., (2012) and this study), the 146-year time interval would allow a strain accumulation of 2.5 to 3.5 m (Table 6). The arguments for an offshore location for the 1766 are mainly based on the inference that this value is nearly half the maximum offset of the 1912 (5.5 m; Altınok et al., 2003). It should be noted that an inland location may be possible if the earthquakes along the Ganos fault are not characteristic and coseismic slip varies among subsequent events. However, we know from the trenches at Güzelköy and Saros that each of the last two events produced 4 to 5 m displacements. Therefore, we have more reasons to consider a characteristic slip model along the offshore-inshore Ganos fault. 4) Both scenarios yield a recurrence interval of 283 years with a deviation of ±81 yr for Scn-1 and ±111 for Scn-2. These are comparable results with Rockwell et al. (2009) and Meghraoui et al. (2012); 280 ±110 years and 323 ±142 years.

Slip rate estimations along the Ganos fault

The 3D paleoseismology studies provide constraints on the slip rate of the North Anatolian Fault. Using a paleo-channel and stream offsets Meghraoui et al. (2012) calculated a slip rate of 17 ± 5 mm/year for the last three events, in the last 1000 years. The trenching revealed a quasicharacteristic faulting behavior with 5 to 6 m coseismic slip per event. Rockwell et al. (2009) determined a 9 m lateral offset on a feeder channel and calculated a slip
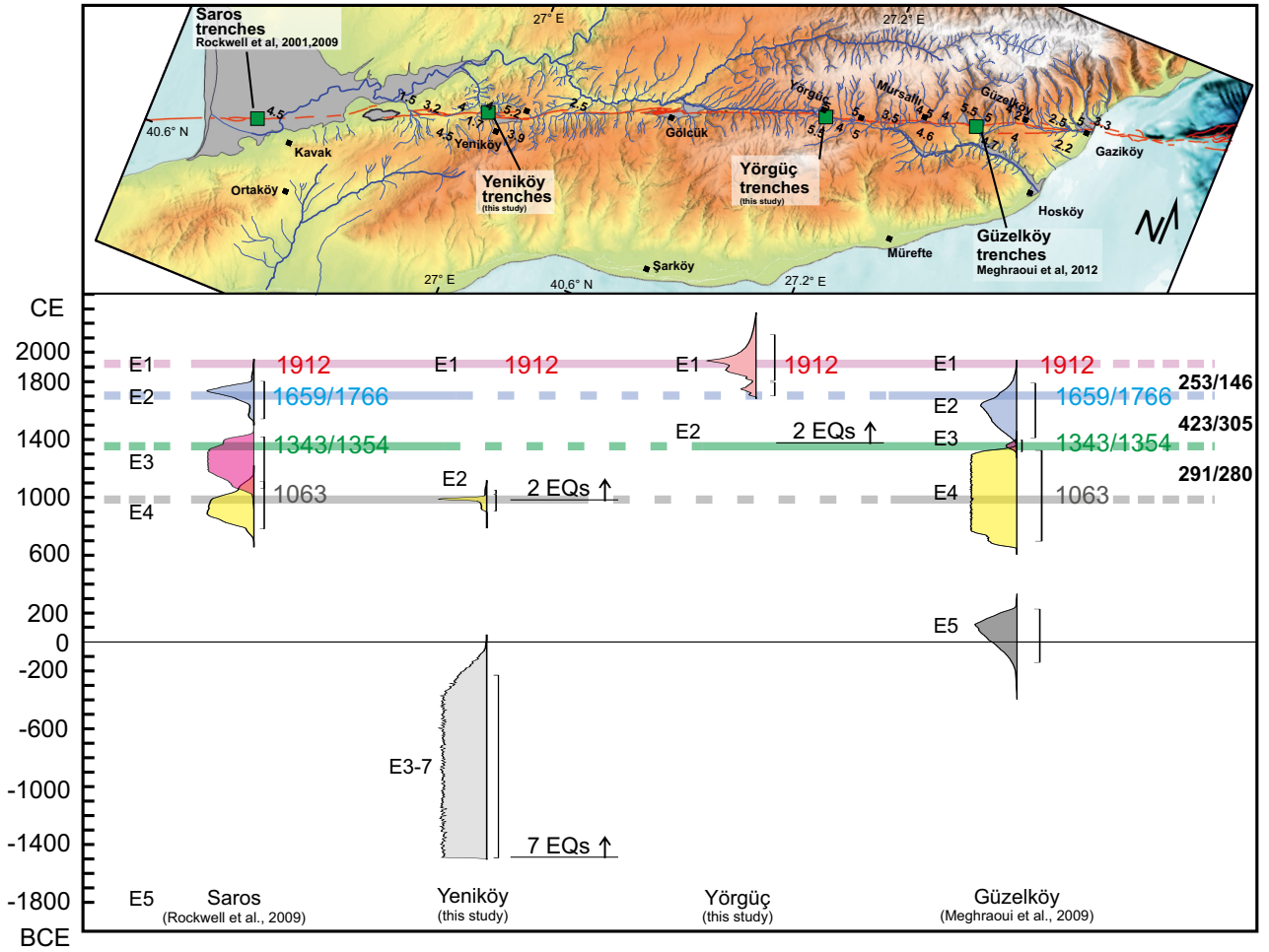
Figure 11. Correlation between this and earlier paleoseismic trench results and spatio-temporal analysis for past large earthquake distributions along the Ganos fault.

Table 5. Considering the last 4 events observed in the trenches confronted to a historical catalog analysis, we suggest two earthquake recurrence scenarios. Taking into account the paleoseismic interseismic periods, Scenario 1 favors a characteristic behavior compared to scenario 2. In Scenario 2, the interseismic periods vary from 146 to 418 years suggesting a noncharacteristic fault behavior. In Scenario 1, the variation of interseismic period is between 253 and 310 years.

Table 6. The upper table summarizes the stored slip for the calculated recurrence interval under different slip rates including the GPS velocities (24 mm/year; Reilinger et al., 2006). The lower section shows the required time period for accumulating given coseismic slips.

Scenario 1		Scenario 2	
Earthquakes (date)	Interval (years)	Earthquakes (date)	Interval (years)
1063		1063	
1343/1354	*286 ±6*	1343/1354	*286 ±6*
1659	*310 ±6*	1766	*418 ±6*
1912	*253*	1912	*146*
Mean recurrence:	*283 ± 81*	*Mean recurrence:*	*283 ± 111*

Recurrence interval	Accumulated slip for 17 mm/year	Accumulated slip for 24 mm/year
283 years	4.8 m	6.8 m
Characteristic co-seismic slip	Geologic slip rate (17 mm/year)	Geodetic velocity (24 mm/year)
5.5 m (max)	324 years	229 years
2.5 m (mean)	146 years	104 years
2.0 m (mean)	118 years	83 years

rate of approximately 16 mm/year for the last two events, also in favor of characteristic slip. Gasperini et al. (2011)

document cumulative offsets of abandoned canyons within the Gulf of Saros and Gulf of İzmit, correlates them with sea level changes related to the Last Glacial Maximum (LGM) and suggests 10 mm/year slip-rate. These values are significantly lower compared to inland paleoseismological slip-rates estimations and are probably because the LGM provides a maximum age for these displacements.

In our case, at Yeniköy, dating the lowermost units of the 46 ± 1 m offset stream channel provided a maximum 16.9 ± 0.7 mm/year slip rate for the last 2732 years.

Combining all three slip rate estimations yields an average right-lateral slip rate of 17.1 ± 0.9 mm/year (Figure 12). The results of the three sites are comparable and consistent along the fault. Necessarily, the cumulative and coseismic fault slips are nearly equally distributed along the inland section.

The Ganos fault runs through an almost homogenous lithology in the Ganos area (Neogene turbiditic units). The fault geometry is simple, linear, and almost continuous. There are minor step-overs and bends along the fault suggesting the absence of any complexity and asperity at depth. The comparable slip rates show a homogenously distributed deformation and are an indirect expression of the geometrical simplicity of the fault towards depth. The absence of post-1912 seismicity along this section is related to this simple fault geometry and the limit of the aseismic section likely marks the extent of the 1912 rupture. In the West and East, the instrumental period earthquakes are concentrated where the fault bifurcates or bends, respectively.

The comparison between the paleoseismic results and GPS velocities shows a clear deficit of the geological fault slip. Hence, more coseismic slip is needed and the attempt to reconcile the two fault slip rates is pointless here. The

slip deficit is a marker for the missing coseismic slip and a parameter for an earthquake forecast (Meghraoui et al., 2021).

6. Conclusion

Our study at Yörgüç shows evidence of two faulting events post-1669 CE ±30 years. At Yeniköy, we determined two faulting events in the last 1000 years and at least 7 events in the last 3500 years. In addition, we succeeded dating a stream channel that was right-laterally offset for 46 ± 1 m. Radiocarbon dating of the base of the stream channel yields a minimum age of 2732 ± 119 years for the channel and implies a maximum slip-rate of 16.9 ± 0.7 mm/year for this section of the Ganos fault. Together with earlier slip-rate estimations, we deduce a 17.1 ± 0.9 mm/year slip rate for the western tip of the North Anatolian fault.

Considering earlier paleoseismic studies, we conclude that the Ganos fault has ruptured during the 1063, 1343a or 1354, 1659 or 1766b, and the 1912 earthquakes. This outcome suggests a recurrence interval of approximately 283 years. Trenching results on the coseismic displacement for the last three events support characteristic slip behavior of 4.5 to 5 m per event. Therefore, we suggest that the 1659 event is more likely to have ruptured the inland Ganos fault and that the 1766b rupture lies further east in the Sea of Marmara.
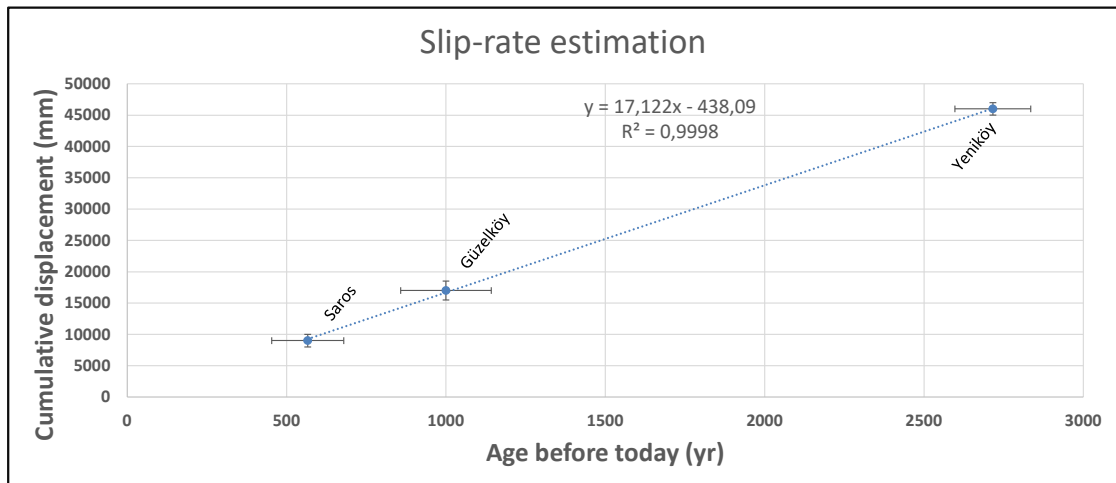
Figure 12. Combining the slip rate estimations from earlier studies, the average short-term paleoseismic slip rate along the Ganos fault is 17.1 ± 0.9 mm/year.

# References

Aksoy ME (2009). Active Tectonics and Paleoseismology of the Ganos Fault Segment and Seismic Characteristics of the 9 August 1912 Mürefte Earthquake of the North Anatolian Fault (Western Turkey). PhD dissertation, Istanbul Technical University, Istanbul.

Aksoy ME (2021). The 9 August 1912 Mürefte-Şarköy earthquake of the North Anatolian fault. Mediterranean Geoscience Reviews 3: 95-114. https://doi.org/10.1007/s42990-021-00050-z

Aksoy ME, Meghraoui M, Polonia A, Çağatay MN, Yavuzoğlu AZ et al. (2022). Subaqueous fault scarps of the North Anatolian Fault in the Gulf of Saros (NE Aegean); where is the western limit of the 1912 Mürefte-Şarköy earthquake rupture? Geophysical Journal International 229: 589-604. https://doi.org/10.1093/gji/ggab462

Aksoy ME, Meghraoui M, Vallee M, Çakır Z (2010). Rupture characteristics of the A.D. 1912 Murefte (Ganos) earthquake segment of the North Anatolian fault (western Turkey). Geology 38: 991-994. https://DOI: 10.1130/G31447.1

Allen CG (1913). Review: Il Disastroso Terremoto nel Bacino Occidental del mar di Marmara: by G. Agamennone. Seismological Society of America 3: 93-94.

Altınok Y, Alpar B, Yaltırak C (2003). Şarköy - Mürefte 1912 Earthquake's Tsunami, extension of the associated faulting in the Marmara Sea, Turkey. Journal of Seismology 7: 329-346. https://doi.org/10.1023/A:1024581022222

Altunel E, Barka AA, Akyüz HS (2000). Slip distribution along the 1912 Mürefte-Şarköy earthquake, the North Anatolian Fault, Western Marmara. In: Barka, A. A., Kozaci, Ö., Akyüz, H. S.&Altunel, E. (eds), Slip distribution along the 1912 Mürefte-Şarköy earthquake, the North Anatolian Fault, Western Marmara. ITU Publications, Istanbul, 341-349.

Altunel E, Meghraoui M, Akyüz HS, Dikbaş A (2004). Characteristics of the 1912 co-seismic rupture along the North Anatolian Fault Zone (Turkey): implications for the expected Marmara earthquake. Terra Nova 16 : 198-204. https://doi.org/10.1111/j.1365-3121.2004.00552.x

Ambraseys NN, Finkel CF (1987). The Saros-Marmara earthquake of 9 August 1912. Earthquake engineering & structural dynamics 15: 189-211. https://doi.org/10.1002/eqe.4290150204

Ambraseys NN (1970). Some characteristic features of the Anatolian fault zone. Tectonophysics 9: 143-165.

Ambraseys NN (2002). The Seismic Activity of the Marmara Sea Region over the Last 2000 Years. Seismological Society of America 92: 1-18. https://doi.org/10.1785/0120000843

Ambraseys NN (2009). Earthquakes in the Mediterranean and Middle East: a multidisciplinary study of seismicity up to 1900. Cambridge University Press, https://doi.org/10.1017/CBO9781139195430

Armijo R, Meyer B, Hubert A, Barka A (1999). Westward propagation of the North Anatolian fault into the northern Aegean: Timing and kinematics. Geology 27: 267-270. https://doi.org/10.1130/0091-7613(1999)027%3C0267:WPOTNA%3E2.3.CO;2

Armijo R, Pondard N, Meyer B, Uçarkus G, Lepinay BM et al. (2005). Submarine fault scarps in the Sea of Marmara pull-apart (North Anatolian Fault): Implications for seismic hazard in Istanbul. Geochemistry Geophysics Geosystems 6: Q06009. https://doi.org/10.1029/2004GC000896

Atakan K, Sorensen MB (2002). Large earthquake faulting and implications for seismic hazard assesment in europe: The izmit-duzce earthquake sequence of august-november 1999 (turkey, mw 7.4,7.1). Technical report, Institutt for Geovitenskap, Universitetet i Bergen.

Barka A (1992). The North Anatolian fault zone. Annales Tectonicae 6: 164-195.

Barka A (1996). Slip distribution along the North Anatolian fault associated with the large earthquakes of the period 1939 to 1967. Seismological Society of America 86: 1238-1254.

Barka A (1999). The 17 August 1999 Izmit Earthquake. Science 285: 1858-1859. https://doi.org/10.1126/science.285.5435.1858

Barka A, Akyüz HS, Altunel E, Sunal G, Çakır Z et al. (2002). The Surface Rupture and Slip Distribution of the 17 August 1999 Izmit Earthquake (M 7.4), North Anatolian Fault. Seismological Society of America 92: 43-60. https://doi.org/10.1785/0120000841

Bronk Ramsey C (2009). Bayesian analysis of radiocarbon dates. Radiocarbon 51: 337-360.

Çakır Z, Chabalier JB, d Armijo R, Meyer B, Barka A et al. (2003). Coseismic and early post-seismic slip associated with the 1999 Izmit earthquake (Turkey), from SAR interferometry and tectonic field observations. Geophysical Journal International 155: 93-110. https://doi.org/10.1046/j.1365-246X.2003.02001.x

Gasperini L, Polonia A, Çağatay MN, Bortoluzzi G, Ferrante V (2011). Geological slip rates along the North Anatolian Fault in the Marmara region. Tectonics 30(TC6001): 1-14. https://doi.org/10.1029/2011TC002906

Guidoboni E, Comastri A (2005). Catalogue of earthquakes and tsunamis in the Mediterranean area from the 11th to the 15th century. Istituto Nazionale di Geofisica e Vulcanologia, Rome.

Guidoboni E, Comastri A, Traina G (1994). Catalogue of ancient earthquakes in the Mediterranean area up to the 10th century. Istituto Nazionale di Geofisica e Vulcanologia, Rome.

Hecker O (1920). Mitteilungen über Erdbeben im Jahre 1912. Editor: Sieberg, A., Hauptstation für Erdbebenforschung, Jena, früher in Strassburg.p.26

Karabulut H, Roumelioti Z, Benetatos C, Ahu Kömec M, Özalaybey S (2006). A source study of the 6 July 2003 (Mw 5.7) earthquake sequence in the Gulf of Saros (Northern Aegean Sea): Seismological evidence for the western continuation of the Ganos fault. Tectonophysics 412: 195-216. https://doi.org/10.1016/j.tecto.2005.09.009

Ketin I (1948). Über die tektonisch-mechanischen Folgerungen aus den großen anatolischen Erdbeben des letzten Dezenniums. Geologische Rundschau 36: 77-83. https://doi.org/10.1007/BF01791916

Ketin I (1969). Uber die nordanatolische Horizontalverschiebung. Bulletin of the Mineral Research and Exploration 1-28.

KOERI (2022). Earthquake Catalogue of Regional Earthquake-Tsunami Monitoring Center.

Konca AÖ, Çetin S, Karabulut H, Reilinger R, Doğan U et al. (2018). The 2014, Mw6.9 North Aegean earthquake: seismic and geodetic evidence for coseismic slip on persistent asperities. Geophysical Journal International 213: 1113-1120. https://doi.org/10.1093/gji/ggy049.

Le Pichon X, Chamot-Rooke C, Rangin N, Şengör AMC (2003). The North Anatolian fault in the Sea of Marmara. Journal of Geophysical Research 108: 2179. https://doi.org/101029/2002JB001862

McCalpin J (2009). Paleoseismology. Academic Press, San Diego.

Meghraoui M, Aksoy ME, Akyüz HS, Ferry M, Dikbaş A et al. (2012). Paleoseismology of the North Anatolian Fault at Güzelköy (Ganos segment, Turkey): Size and recurrence time of earthquake ruptures west of the Sea of Marmara. Geochemistry, Geophysics, Geosystems 13: Q04005-Q04005. https://doi.org/10.1029/2011GC003960

Meghraoui M, Toussaint R, Aksoy ME (2021). The slip deficit on the North Anatolian Fault (Turkey) in the Marmara Sea: insights from paleoseismicity, seismicity and geodetic data. Mediterranean Geoscince Reviews 3: 45-56. https://doi.org/10.1007/s42990-021-00053-w

Mihailovic J (1927). Trusne katastrofe na Mramornome moru sa narocitim pogledom na opstu seizmicnost Mramornoga mora i njegovih obala. Belgrade.

Önder Ş, Görür N, Polonia A, Gasperini L (2021). Fault-controlled gas escapes in the shelf sediments of the Saros Gulf, NE Aegean Sea. Turkish Journal of Earth Sciences 30: 862-881. https://doi.org/10.3906/yer-2107-28

Reilinger RE, McClusky S, Vernant P, Lawrence S, Ergintav S et al. (2006). GPS constraints on continental deformation in the Africa-Arabia-Eurasia continental collision zone and implications for the dynamics of plate interactions. Journal of Geophysical Research 111: https://doi.org/10.1029/2005JB004051

Reimer P Austin W, Bard E, Bayliss A, Blackwell P et al. (2020). The IntCal20 Northern Hemisphere Radiocarbon Age Calibration Curve (0–55 cal kBP). Radiocarbon 62 (4): 725-757. https://doi:10.1017/RDC.2020.41

Rockwell TK, Barka A, Dawson T, Akyüz S, Thorup K (2001). Paleoseismology of the Gazikoy-Saros segment of the North Anatolia fault, northwestern Turkey: Comparison of the historical and paleoseismic records, implications of regional seismic hazard, and models of earthquake recurrence. Journal of Seismology 5: 433-448. https://doi.org/10.1023/A:1011435927983

Rockwell TK, Ragona D, Seitz G, Langridge R, Aksoy ME et al. (2009). Palaeoseismology of the North Anatolian Fault near the Marmara Sea: implications for fault segmentation and seismic hazard. Geological Society, London, Special Publications 316: 31-54. https://doi.org/10.1144/SP316.3

Sadi MDY (1912). Marmara Havzasının 26-27 Temmuz Hareket-i Arzı 15 Eylül 1328. Resimli Kitap Matbaası, İstanbul 45.

Schmittbuhl J, Karabulut H, Lengliné O, Bouchon M (2015). Seismicity distribution and locking depth along the Main Marmara Fault, Turkey. Geochemistry, Geophysics, Geosystems 17: 954-965. https://doi.org/10.1002/2015GC006120

Soysal H, Sipahioğlu S, Kolçak D, Altınok Y (1981). Historical Earthquake Catalogue of Turkey and Surrounding Area (2100 B.C. – 1900 A.D.). TÜBİTAK report no: TBAG-341(in Turkish).

Stein RS, Barka AA, Dieterich JH (1997). Progressive failure on the North Anatolian fault since 1939 by earthquake stress triggering. Geophysical Journal International 128: 594-604. https://doi.org/10.1111/j.1365-246X.1997.tb05321.x

Tamtaş BD, Yalçınkaya E, Görgün E (2021). Ganos Fayı ile Tekirdağ Baseni Arasında Meydana Gelen Mikro Depremlerin Moment Tensör ve Gerilme Analizleri. Turkish Journal of Earthquake Research 3: 167-192. https://dergipark.org.tr/en/pub/tdad/issue/66337/1014479

Taymaz T, Jackson J, McKenzie D (1991). Active tectonics of the north and central Aegean Sea. Geophysical Journal International 106: 433-490. https://doi.org/10.1111/j.1365-246X.1991.tb03906.x

Toksöz MN, Shakal AF, Michael AJ (1979). Space-time migration of earthquakes along the North Anatolian fault zone and seismicity gaps. Pure and Applied Geophysics 117: 1258-1270.

Tüysüz O, Barka A, Yiğitbaş E (1998). Geology of the Saros graben and its implications for the evolution of the North Anatolian fault in the Ganos-Saros region, northwestern Turkey. Tectonophysics 293: 105-126. https://doi.org/10.1016/S0040-1951(98)00085-7

Ustaömer T, Gökaşan E, Tur H, Görüm T, Batuk F et al. (2008). Faulting, mass-wasting and deposition in an active dextral shear zone, the Gulf of Saros and the NE Aegean Sea, NW Turkey. Geo-Marine Letters 28: 171-193. https://doi.org/10.1007/s00367-007-0099-6

Yaltırak C, Alpar B (2002). Kinematics and evolution of the northern branch of the North Anatolian Fault (Ganos Fault) between the Sea of Marmara and the Gulf of Saros. Marine Geology 190: 351-366. https://doi.org/10.1016/S0025-3227(02)00354-7

Supplementary
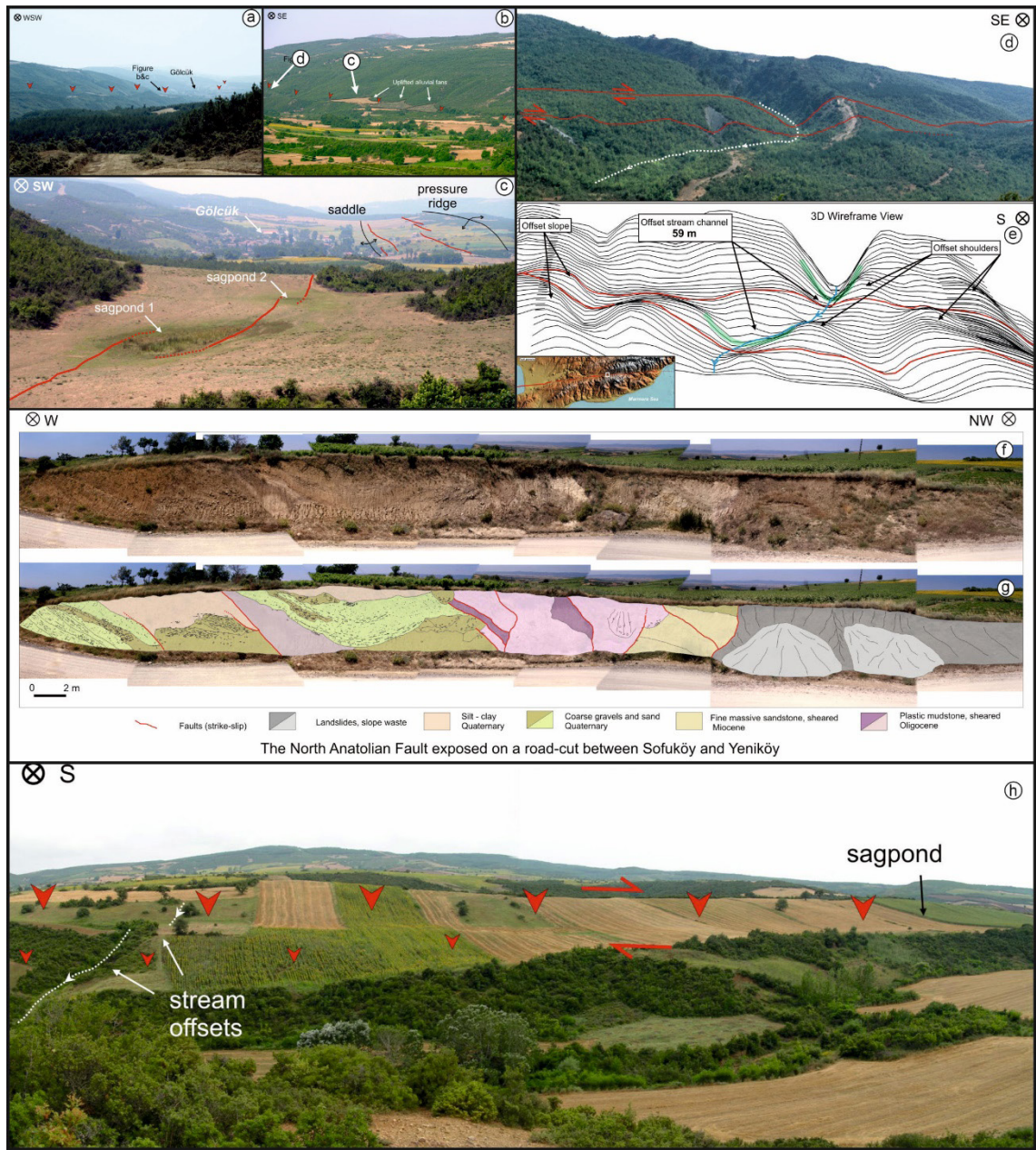
Figure S1. Examples of the geomorphic imprint of the Ganos fault a) Breaks on hill slopes and saddles. b) Three uplifted alluvial fans located east of Gölcük indicate the vertical slip component along the fault. c) Three sag ponds on the fans mark the cumulative deformation of the most recent earthquake ruptures. d and e) East of Gölcük, we measured a 59-m right lateral displacement on a valley running across the fault. f and g) At Yeniköy, a road outcrop truncates Neogene and Quaternary units. Tilted and juxtaposed units expose the most recent deformation. h) West of Yeniköy continuous breaks along slopes, offsets and sag ponds allow locating the Ganos fault.
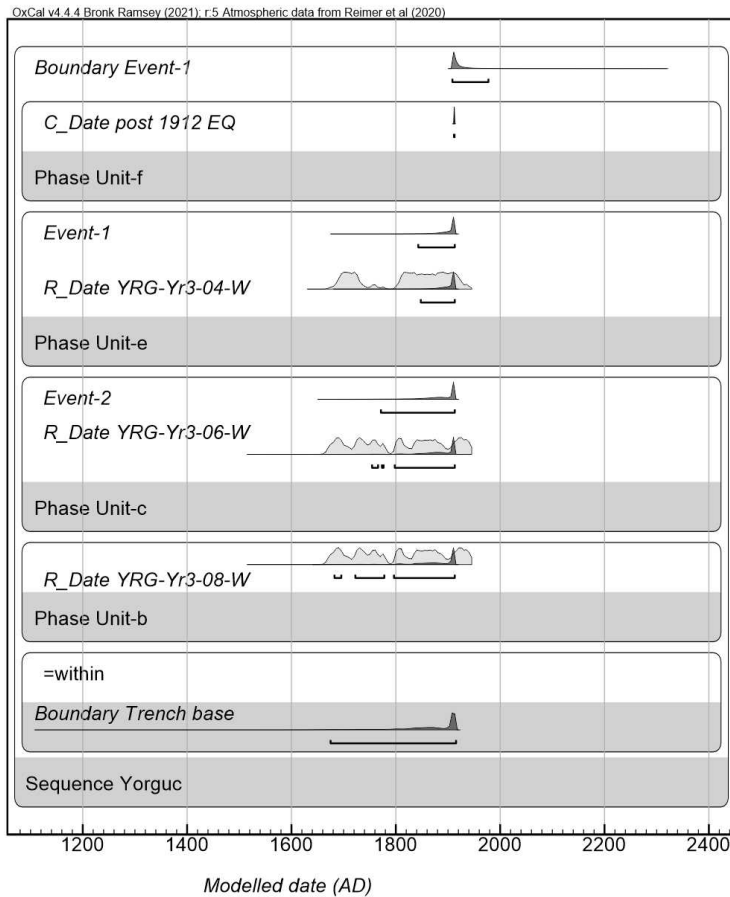
Yörgüç Trenches

Trench Yr2 unit descriptions: Unit-a is made of an unconsolidated yellow-grey silty sand deposit. It interfingers laterally to a greenish-yellow sandy-silty clay unit-b. Unit-b interfingers towards south with unit-c which is a greenish clay deposit. A brown silty clay unit (d)

deposits on top of these units with an erosional base. Unit-d is overlain with unit-e which is a brownish-grey clay deposit. The base of unit-e is also erosional and is overlain on the top by soil.

Trench Yr3 unit descriptions: The lowermost unit consists of yellow clayey silt with scattered coarse gravels (unit-a). Unit-b is similar to unit-a; however, the amount of gravel is significantly less. The unit is overlain by a brownish silty clay on top of an erosional surface. The upper units e and f show intercalation with seasonal variation in deposition. Both units are rich in organic material and bear bioturbation. The sequence is truncated by a colluvial deposit (unit-g), which is overlain by soil containing fine grains.

Table S1. In Yr3 of Yörgüç, we identify eight deposits with different sedimentary content.

| Unit	Description
s	Soil
g	Light brown clayey silt, consolidated
f	Yellow silty fine sand
e	Greenish-brown clay with mica and silt, consolidated
d	Yellow silt with mica content
c	Brownish, dark grey silty clay
b	Yellow clayey silt with a few scattered gravels. Clasts contain mica.
a	Yellow clayey silt with abundant scattered coarse gravels.

Figure S2. Oxcal plot of the probability density functions (PDF) for radiocarbon samples from the Yörgüç trench Yr3 (Bronk Ramsey 2021). The IntCal20 curve is used for calibration (Reimer et al. 2020). The multiplot simulates the time range of the faulting events.
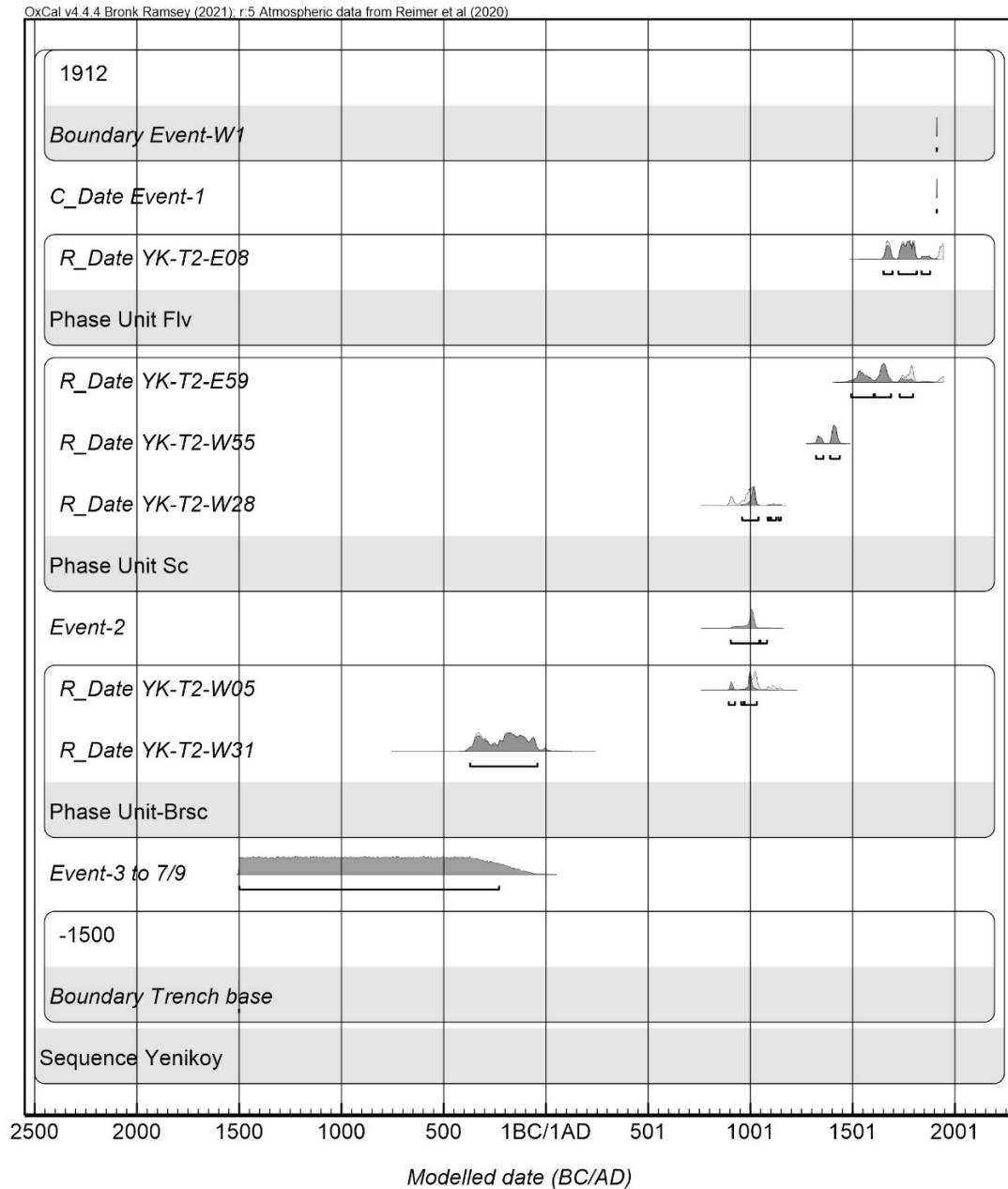
Yeniköy Trenches

Table S2. List of stratigraphic units exposed on the Yeniköy trench walls and their lithologic descriptions.

Trench	Unit	Description	
T1	f_2	Soil with coarse grains	
	f_1	Soil with fine grains	
	e	Coarse to fine, well sorted medium rounded clasts forming a typical sequence of fluvial stratigraphy with horizontal- and cross-bedding and channel)	subunits of the alluvial package
	d	Stratified grey clayey silt, interfingering with unit-f .	
	c	Bluish-grey silty clay with scattered gravel content	
	b	Reddish oxidized clay with silt and callish	
	a	Grey silt clay with very coarse gravels	
	a_3	Light-grey silt and clay	sub-units of a colluvial package
	a_2	Yellow silty clay	
	a_1	Bluish-grey silty clay with coarse gravels	
T2	i	Plow	
	h	Beds of fine gravels, sand, silt and clay. cross-bedding (alluvial)	
	g	Brown-grey clayey silt	
	f	Brown massive clay with very few medium rounded poorly sorted gravel content	
	e	Light yellow, clayey silt with scattered gravels content and some bioturbations	
	d	Reddish oxidized clay with callish	
	c	Silty clay deposits with coarse gravels	
	b	Bluish-grey silty clay with scattered gravel content	
	a	Light brown massive clay with poorly rounded medium sorted scattered gravels.	
T4	f	Reddish clay	
	e	Light grey – brown silty clay	
	d	Dark brown – grey silty clay	
	c	Grey – green clayey fine sand (alluvial)	
	b	Massive clay with scattered gravels and very large clasts (colluvium)	
	a	Light brown massive clay with poorly rounded medium sorted scattered gravels.	
T5	e	Grey – yellow clay and silt mixed with medium size gravels	
	d	Grey – yellow clay and silt with medium size gravels, stratified.	
	c_3	Grey massive cemented silt with thin clay layer and some gravels	
	c_2	Coarse to fine, well sorted medium rounded consolidated clasts with horizontal- and cross-bedding and channels	sub-units of the alluvial package
	c_1	Reddish massive silty clay with increasing silt content towards east	
	b	Massive clay with scattered gravels and very large clasts (colluvium)	
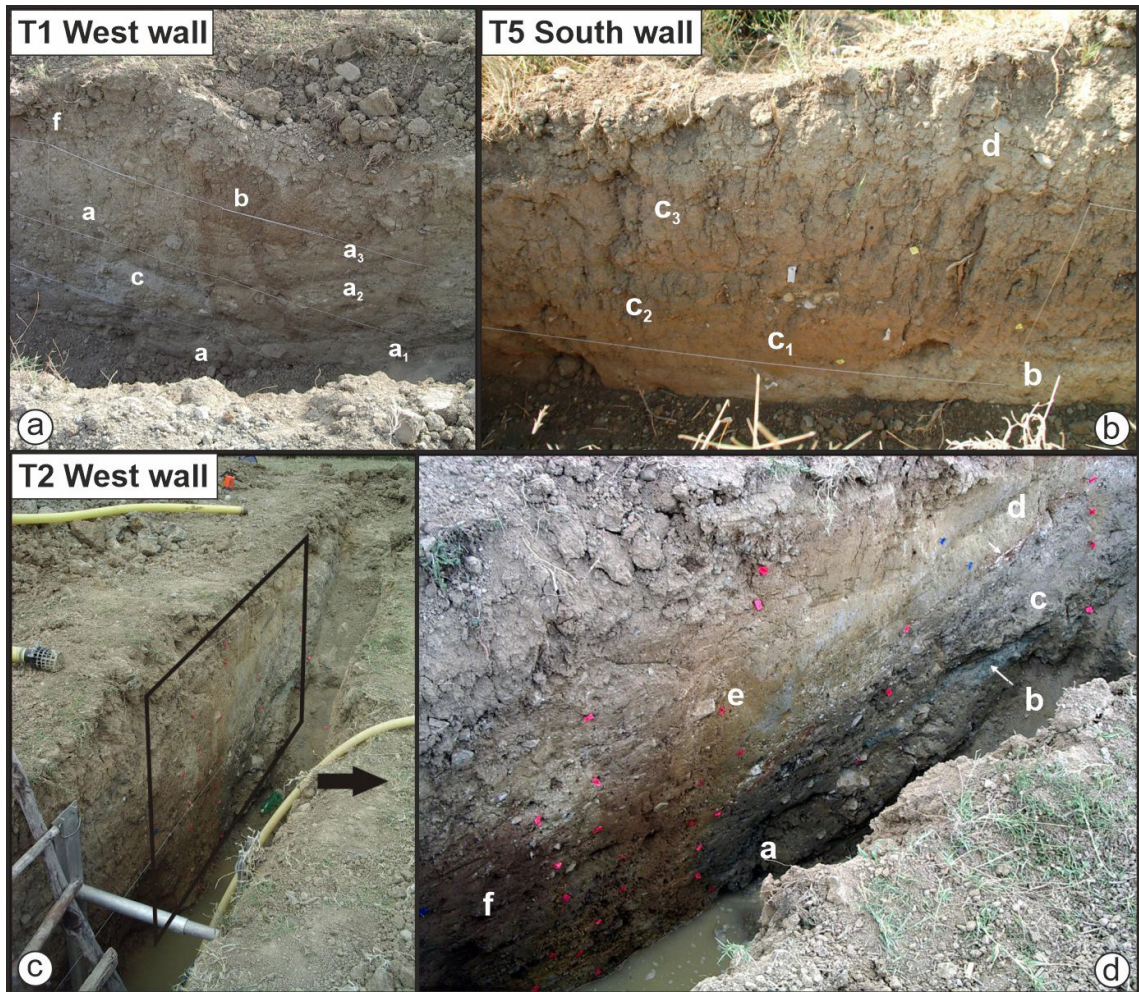
Figure S3. a) and b) show the fault zone in T2. Red flags mark the faults. c) West trench wall of T1. Reddish-brown vertical zones correspond to fault splays (see arrows). d) Deposits Fac, Fbc, Fgs, and Col of the Köy creek are exposed in T5. The sediments are deposited on top of a base made of colluvium.

Figure S4. Oxcal plot of the probability density functions (PDF) for selected radiocarbon samples from the Yeniköy trenches (Bronk Ramsey 2021). The IntCal20 curve is used for calibration (Reimer et al. 2020). The multiplot simulates the time range of the faulting events.
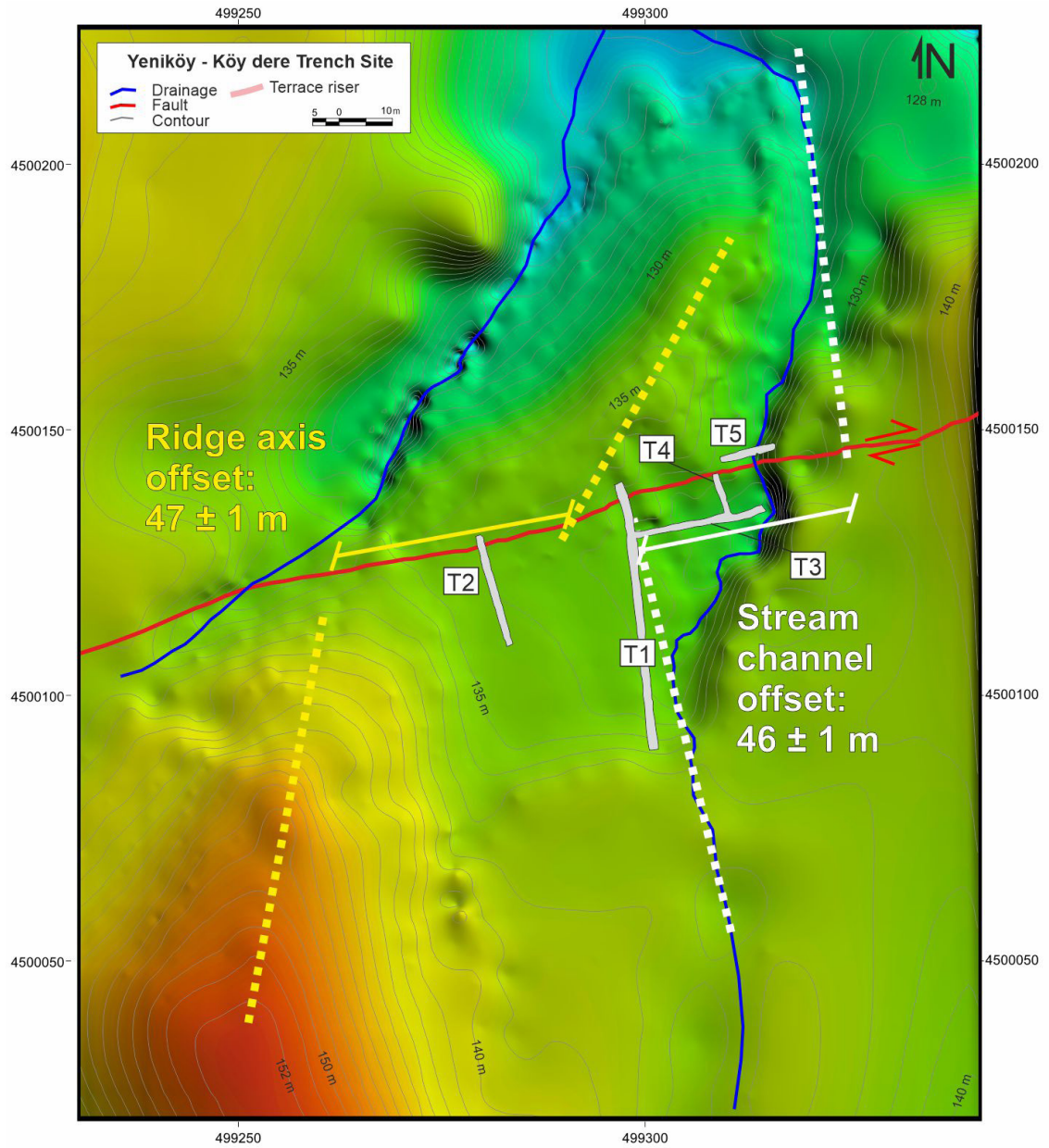
Figure S5. The digital elevation model of the site (obtained from 5500 Total Station measurements; coordinates are UTM ED50 Zone 35N). On-site and remote measurements from the plot yield comparable 47 ± 1 m and 46 ± 1 m right lateral fault displacement along strike for the ridge axis and the stream channel, respectively.